
RETHINKING GRAPH STRUCTURE LEARNING IN THE ERA OF LLMs

A PREPRINT

Zhihan Zhang*

Department of Computer Science and Technology
Beijing Institute of Technology
Beijing 100081, China
3220241443@bit.edu.cn

Xunkai Li*

Department of Computer Science and Technology
Beijing Institute of Technology
Beijing 100081, China
cs.xunkai.li@gmail.com

Guang Zeng

Department of Computer Science and Technology
Ant Group
Beijing 100081, China
zengguang_77@qq.com

Hongchao Qin

Department of Computer Science and Technology
Beijing Institute of Technology
Beijing 100081, China
qhc.neu@gmail.com

Rong-Hua Li†

Department of Computer Science and Technology
Beijing Institute of Technology
Beijing 100081, China
lironghuabit@126.com

Guoren Wang

Department of Computer Science and Technology
Beijing Institute of Technology
Beijing 100081, China
wanggrbit@gmail.com

April 29, 2025

ABSTRACT

Recently, the emergence of LLMs has prompted researchers to integrate language descriptions into graphs, aiming to enhance model encoding capabilities from a data-centric perspective. This graph representation is called text-attributed graphs (TAGs). A review of prior advancements highlights that graph structure learning (GSL) is a pivotal technique for improving data utility, making it highly relevant to efficient TAG learning. However, most GSL methods are tailored for traditional graphs without textual information, underscoring the necessity of developing a new GSL paradigm. Despite clear motivations, it remains challenging: (1) How can we define a reasonable optimization objective for GSL in the era of LLMs, considering the massive parameters in LLM? (2) How can we design an efficient model architecture that enables seamless integration of LLM for this optimization objective? For Question 1, we reformulate existing GSL optimization objectives as a tree optimization framework, shifting the focus from obtaining a well-trained edge predictor to a language-aware tree sampler. For Question 2, we propose decoupled and training-free model design principles for LLM integration, shifting the focus from computation-intensive fine-tuning to more efficient inference. Based on this, we propose Large Language and Tree Assistant (LLaTA), which leverages tree-based LLM in-context learning to enhance the understanding of topology and text, enabling reliable inference and generating improved graph structure. Extensive experiments on 10 datasets demonstrate that LLaTA enjoys flexibility-incorporated with any backbone; scalability-outperforms other LLM-enhanced graph learning methods; effectiveness-achieves SOTA predictive performance.

*These authors contributed equally to this work.

†Corresponding author.

1 Introduction

In recent years, the rise of LLMs in graph ML [29, 3] has led to the emergence of text-attributed graphs (TAGs) as a novel data representation. This data structure leverages textual information to provide fine-grained descriptions of graphs, driving a significant shift in data-centric graph learning [15]. Inspired by this, efficiently and robustly learning TAGs has become an urgent priority.

To achieve this, graph structure learning (GSL) is a promising approach that enhances data utility for vanilla graph neural networks (GNNs). However, most existing prevalent GSL approaches [35] are designed for traditional graphs and fail to process rich textual information, leading to sub-optimal performance. Despite significant efforts by recent LLM-based GSL methods, such as GraphEdit [7] and LLM4RGNN [31], their optimization objectives and model architectures still adhere to traditional GSL paradigms, inheriting unnecessary complexities. Specifically, these prominent GSL approaches [32, 28, 10, 7, 31] rely on carefully designed loss functions to dynamically maintain a graph learner (i.e., structure optimizer) coupled with well-defined instruction datasets or a specific GNN backbone (i.e., improved structure tailored for the specific downstream encoder). Based on this, we have the following 2 observations and seek to explore them to gain key insights into developing a new GSL paradigm in the era of LLMs.

Observation 1 (Optimization Objective): The graph learner often serves as an edge predictor, heavily relying on end-to-end training with a specific downstream backbone. In the era of LLMs, LLMs will play a crucial role in graph learners. In this context, performing full-parameter LLM training to obtain an edge predictor is infeasible. While two recent fine-tuning methods have been proposed, the complexity of constructing instruction datasets and tuning still hinders their efficiency. This leads to **Question 1**: How can we define a reasonable optimization objective for LLM-enhanced GSL?

Answer 1: In Sec. 3.1, we present a new *optimization framework* that reformulates the existing GSL optimization objective (well-trained edge predictor) as a tree-based optimization task (well-defined language-aware tree sampler).

Observation 2 (Model Architecture): To obtain a well-trained edge predictor, the existing graph learner is often coupled with customized instruction datasets or a specific graph learning backbone, with gradient supervision for model parameter updates in a collaborative manner. The complexity of this model architecture hinders the adaptability of the improved graph structure to real-world scenarios (i.e., deployment efficiency, instruction-free, and backbone-free). In the era of LLMs, LLMs possess remarkable in-context learning capability with textual information, paving the way for efficiently obtaining improved structure. Based on this and Observation 1, we adopt a tree-oriented in-context learning approach. However, we must address **Question 2**: How can LLM be seamlessly integrated into the model architecture for efficient GSL?

Answer 2: In Sec. 3.2, we establish the *decoupled and training-free model design principles* by revisiting existing GSL, emphasizing efficient LLM inference over computation-intensive fine-tuning.

Based on the aforementioned key insights from Answers, we propose Large Language and Tree Assistant (LLaTA) as follows: (1) **Topology-aware In-context Construction**: We first quantify the dynamic complexity of graph topology via structural entropy. By employing the greedy algorithm to minimize this measurement, we construct a hierarchical structural encoding tree, which captures topology insights centered on multi-level communities (i.e., non-leaf nodes within the tree). (2) **Tree-prompted LLM Inference**: Subsequently, this tree serves as a high-quality prompt, enabling LLMs to perform in-context learning for a comprehensive understanding of topology and text. Specifically, we utilize LLM to reveal textual semantic relationships within the leaf community. Based on these topology and text insights, we reallocate the leaf dependency to achieve tree optimization. (3) **Leaf-oriented Two-step Sampling**: Finally, we perform an LLM-guided leaf selection to identify the current node and candidate nodes for edge addition or removal, enabling training-free GSL. The core idea of LLaTA is to enable LLM in-context learning through topology-aware tree prompts, eliminating the need for expensive fine-tuning. In Sec. 3.3, we provide the empirical investigation, demonstrating the effectiveness of this new GSL paradigm in the era of LLMs.

Our contributions. (1) *New Perspective*. We systematically review existing GSL methods and provide empirical investigations, revealing the challenges and opportunities for GSL in the era of LLMs. (2) *Innovative Approach*. We reformulate the existing GSL and propose a tree-based optimization framework with model design principles. Based on this, we introduce LLaTA, which seamlessly integrates both topology and text insights by tree-driven prompts to facilitate LLM in-context learning and generate improved graph structure, with complete theoretical support. (3) *SOTA Performance*. Extensive experiments demonstrate the superior performance of LLaTA. It outperforms recent LLM-based methods by 1.3%-2.5% in accuracy while running 3.0h-9.7h faster.

2 Preliminaries

2.1 Notations and Problem Formulation

Node-wise Text-Attributed Graph. In this paper, we consider a TAG $\mathcal{G} = (\mathcal{V}, \mathcal{E})$ with $|\mathcal{V}| = n$ nodes, $|\mathcal{E}| = m$ edges. It can be described by a symmetrical adjacency matrix $\mathbf{A}(u, v)$. Each node has a feature vector of size f and a one-hot label of size c , the feature and label matrix are represented as $\mathbf{X} \in \mathbb{R}^{n \times f}$ and $\mathbf{Y} \in \mathbb{R}^{n \times c}$. Meanwhile, \mathcal{G} has node-oriented language descriptions, which are represented as $t_i \in \mathcal{T}$ for each node and associated with its features x_i .

Graph Structure Learning in TAGs. In this paper, we aim to improve the graph structure \mathbf{A}^* for any downstream task by incorporating original topology and textual information. Given the output predictions $\hat{\mathbf{Y}}$ from the downstream backbone with improved structure, the general loss is formulated as $\mathcal{L}_{\text{task}}(\hat{\mathbf{Y}}, \mathbf{Y}) + \alpha \mathcal{L}_{\text{reg}}(\mathbf{A}^*, \mathbf{A})$, where $\mathcal{L}_{\text{task}}$ evaluates specific task performance (e.g., node classification), and \mathcal{L}_{reg} establishes the guiding principles for improved structure.

2.2 Complexity Metrics of Graph Topology

Structural Entropy. Motivated by Shannon entropy [23], structural entropy (SE) [13] is an effective measurement for quantifying the dynamic complexity of graph topology. By minimizing SE, we can reduce structure uncertainty and capture inherent patterns, thereby supporting downstream tasks in a robust and interpretable manner. In other words, this approach uncovers meaningful structural patterns and ensures that it aligns more effectively with task-specific requirements. This has made it a pivotal tool for GNNs, gaining significant attention in recent years.

Structural Encoding Tree. By minimizing SE using the greedy algorithm, we can construct a structural encoding tree \mathcal{T} . This tree reorganizes the original graph and simulates the natural evolution of the graph through its inherent hierarchical structure. Specifically, its leaf nodes correspond to the original graph nodes, and non-leaf nodes represent multi-level communities. Low-level communities capture connected leaf nodes with high homophily, while higher levels reflect unseen structural patterns. It offers GSL a new perspective. More details can be found in Appendix A-B.

2.3 Related Works

SE-based Methods. Existing SE-based methods leverage the well-defined structural encoding tree to perform a wide range of graph-based downstream tasks such as node clustering [22], community detection [17], multi-layer coarsening [27], and embedding dimension estimation [30]. Recent SEGSL [37] enhances edge connectivity and quality using this structural encoding tree, but it relies on end-to-end tree-based training without incorporating LLMs.

Traditional GSL. These methods can be categorized into metric-based [2, 14, 28], probabilistic sampling [32, 19, 16], and directly learnable methods [11, 18]. Specifically, they refine graph structure using well-designed measurement (e.g., homophily and connectivity), edge re-weight, random sampling, or direct topology optimization without textual information.

LLM-based GSL. GraphEdit [7] improves node connectivity by adding neighbors through a well-trained edge predictor and refines the improved graph structure by evaluating node relevance using a fine-tuned LLM. LLM4RGNN [31] leverages a fine-tuned LLM to infer node relevance, which is used to train an edge predictor. Compared to improving the graph structure, it focuses more on robustness against graph adversarial attacks.

3 GSL in the Era of LLMs

3.1 GSL Optimization Objectives Reformulation

As highlighted by Obs.1 in Sec. 1, existing GSL methods aim to train an effective edge predictor as the graph learner. This typically requires coupling the graph learner with a specific backbone and jointly optimizing them. Although effective, this objective becomes inefficient for LLMs due to their large number of parameters. Our investigation shows that current LLM-based GSL approaches often adopt instruction fine-tuning to mitigate full-parameter training. However, understanding complex graph structures and crafting appropriate instruction datasets can be labor-intensive, as reflected in their elaborate workflows [7, 31]. To address this, we reformulate GSL and introduce a tree-based optimization framework that avoids edge predictors, as illustrated in Fig. 1 (a)-(c). The core idea is to develop a language-aware tree sampler for efficient GSL.

Specifically, (a) Tree Construction first reorganizes the original graph to assist LLMs in understanding the topology. Based on this, (b) Tree Optimization leverages textual information and LLM to perform tree optimization. Finally, (c) Improved Structure is generated by a language-aware tree sampler. Please refer to Sec.3.2 and Sec.4 for implementation of the above framework in LLaTA.

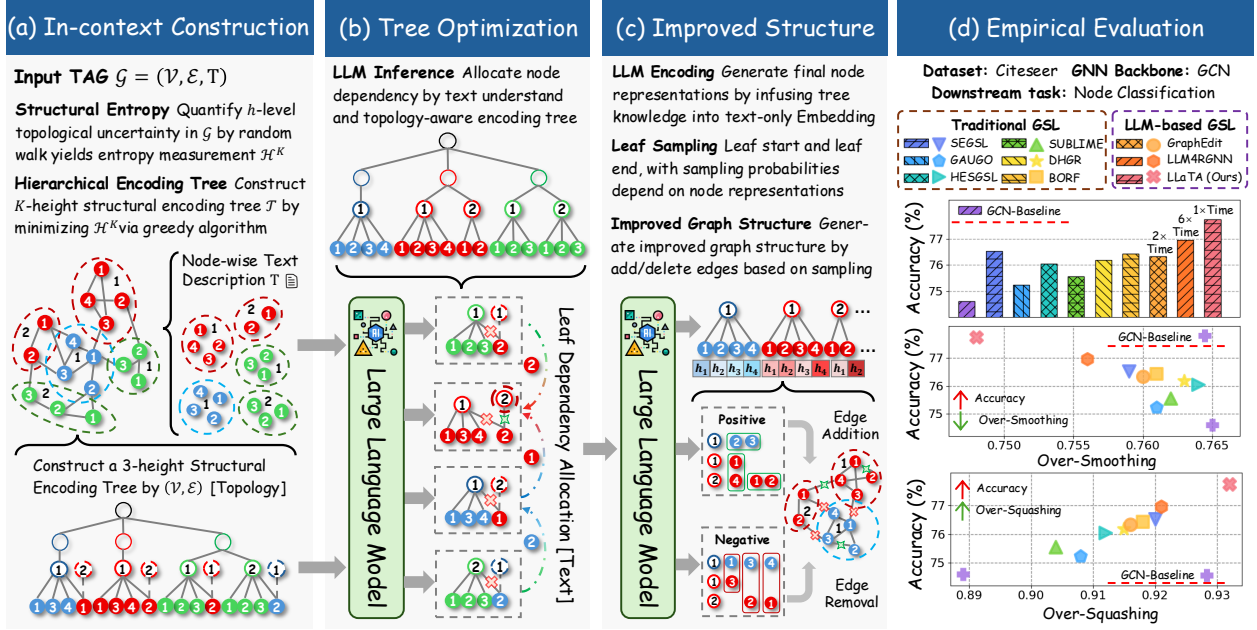


Figure 1: The overview of our proposed tree-based GSL optimization pipeline and empirical results.

3.2 Model Architecture Review

As outlined by Obs. 2 in Sec. 1, integrating LLMs in GSL remains a challenge. To establish model design principles for tree optimization, we revisit existing GSL paradigms.

The **Coupled Paradigm** tightly integrates the graph learner and backbone for task-specific learning. However, it faces limitations such as unstable performance due to restricted generalizability and fairness concerns, and inflexible deployment as switching tasks or backbones requires retraining. In contrast, the **Decoupled Paradigm** trains the graph learner and backbone independently, offering better compatibility with LLMs for GSL. Although recent LLM-based GSL methods adopt this approach, they still face challenges such as indirect integration of topology and text, reliance on instruction datasets, and the complexity of fine-tuning. For a more efficient and reliable approach, we recommend a fully decoupled paradigm, reducing fine-tuning reliance and focusing on high-quality in-context prompts. Detailed discussion is provided in the Appendix C.

To achieve this, we leverage the in-context learning ability of LLMs to jointly understand graph topology and node text for reliable inference. Specifically, **(a) Tree Construction**: we first build a structural encoding tree to generate topology-aware in-context prompts, enhancing the LLM’s understanding of graph structure. Then, **(b) Tree Optimization**: based on these prompts, we use LLMs to infer semantic relationships among nodes from their textual descriptions, and reassign leaf dependencies to optimize the tree structure. The resulting hierarchical tree integrates both structural and textual information, forming a strong basis for GSL. Finally, **(c) Improved Structure**: we apply a leaf-oriented two-step sampling to select the current node and a candidate set for edge modification, yielding an improved graph for any downstream scenario. For deeper insights into the leaf-oriented sampler within GSL, please refer to Appendix B.

3.3 Empirical Investigation

To demonstrate the effectiveness of our proposal in Sec. 3.1-3.2, we present empirical results in Fig. 1(d). Due to space constraints, detailed experimental settings and analysis are provided in Appendix D. In our reports, over-smoothing (\downarrow) reflects the distinguishability of node embeddings, while over-squashing (\uparrow) indicates the ability of nodes to perceive distant ones. These metrics are widely used in recent GSL studies to quantify the quality of improved structure, as they not only directly impact downstream accuracy (\uparrow) but also evaluate method robustness. They demonstrate that LLM-based GSL methods generate higher-quality structures than traditional ones, underscoring the necessity of LLMs. Furthermore, LLaTA achieves the best performance, validating the effectiveness of our proposed new GSL paradigm.

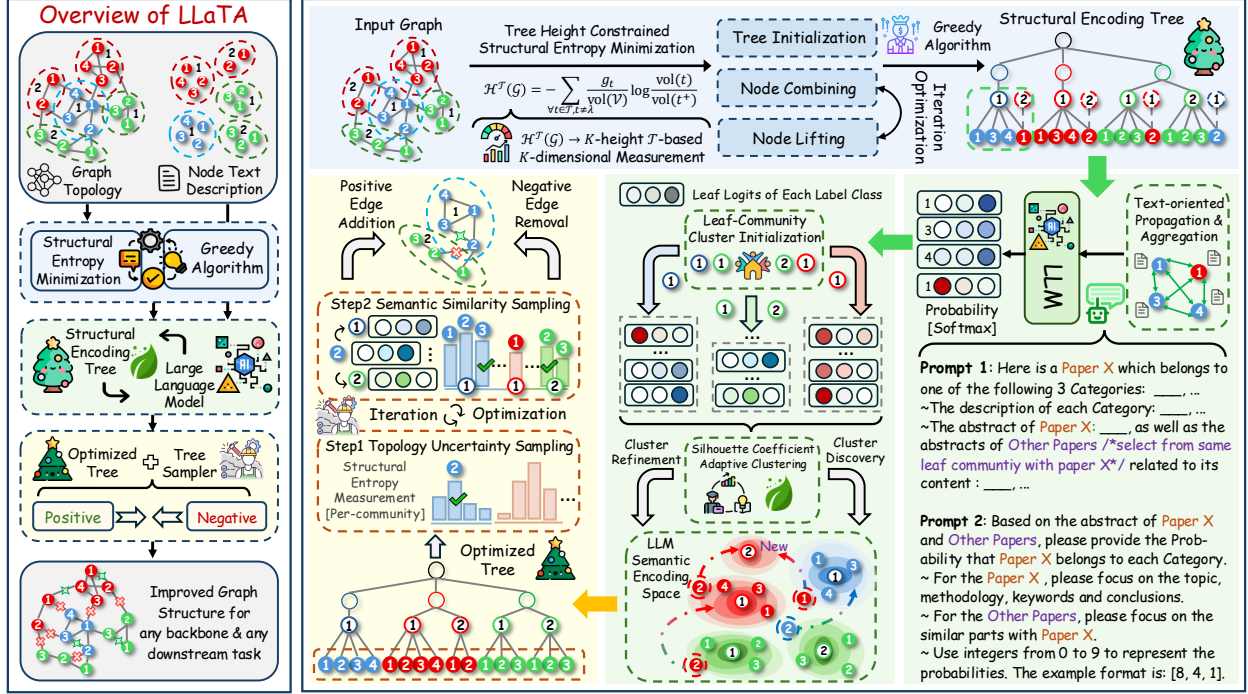


Figure 2: (Left) The overview of LLaTA; (Right) The detailed pipeline of LLaTA, which includes: **topology-aware tree prompts**, **reliable LLM inference** and **language-aware tree sampler**.

4 Our Method

4.1 Overview of LLaTA

We instantiate the three components outlined in Fig. 1 and propose LLaTA, shown in Fig. 2. The correspondences are: (a)-(1) Topology-aware In-context, (b)-(2) Tree-prompted LLM Inference and (c)-(3) Leaf-oriented Two-step Sampling.

4.2 Topology-aware In-context Construction

Motivation. To address the potential performance decline caused by the absence of fine-tuning and obtain reliable inference, we enable efficient in-context learning with high-quality prompts. Based on Sec. 2.2, structural entropy is a promising strategy for constructing these prompts, as it offers an interpretable theory for capturing both local and global topology insights.

To establish a hierarchical encoding tree that simulates the natural evolution of graph topology, we constrain the height of this tree to K and minimize K -dimensional SE proposed by [13]. The optimization objective definition:

$$\mathcal{T}^* = \underset{\mathcal{T}}{\operatorname{argmin}} \mathcal{H}^T(\mathcal{G}), \quad \mathcal{H}^T(\mathcal{G}) = \sum_{\phi \in \mathcal{T}, \phi \neq \lambda} \mathcal{H}^T(\mathcal{G}, \phi) = - \sum_{\phi \in \mathcal{T}, \phi \neq \lambda} \frac{g_\phi}{\operatorname{vol}(\mathcal{G})} \log \frac{\operatorname{vol}(\phi)}{\operatorname{vol}(\phi^+)}, \quad (1)$$

where $\operatorname{vol}(\mathcal{G})$ is the sum of the degrees of all nodes in \mathcal{G} , $\operatorname{vol}(\phi)$ is the sum of the degrees of nodes in ϕ , ϕ^+ is the parent of ϕ , λ is the root node, \mathcal{T}^* denotes the optimized tree that minimizes its structural entropy $\mathcal{H}^T(\mathcal{G})$. We employ a greedy algorithm to minimize the structural entropy $\mathcal{H}^T(\mathcal{G})$ and construct a hierarchical encoding tree \mathcal{T}^* with a predefined height K . The algorithm starts by initializing a tree of height 1, where each graph node is a leaf under a common root. It then iteratively combines node pairs to reduce $\mathcal{H}^T(\mathcal{G})$, followed by node lifting operations to further optimize the structure. The node lifting process continues until the tree height is reduced to K . The full algorithm and the operations involved is detailed in Appendix E.1.

Theorem 1 (Topological Information Capturing Properties of Encoding Tree). *Given an encoding tree \mathcal{T} and a non-leaf node $\phi \in \mathcal{T}$, the error of topological information $\varepsilon^h(\phi)$ in community \mathcal{C}_ϕ is upper bounded by: $\frac{g_\phi}{2m} \log_2 \frac{\operatorname{vol}(\phi^+)}{g_\phi}$, and $\varepsilon^h(\phi)$ gradually decreases as the community level descends.*

Theorem 2 (Implicit Global Constraints in Low-Level Communities). *In a structural encoding tree \mathcal{T} , each low-level community \mathcal{C}^l captures localized topology but implicitly retains global structure constraints due to the hierarchical, random-walk-based formulation of structural entropy.*

Drawing on Theorems 1 and 2, we infer that low-level communities in the encoding tree provide a more faithful representation of the graph’s topology, as they simultaneously preserve local connectivity and global structural constraints. Accordingly, for each leaf node α , we assign its associated low-level community $\mathcal{C}^\ell(\alpha)$ as a topological context to enhance the accuracy of downstream inference by the LLMs. The proof process of Theorems 1 and 2 is provided in Appendix F.1-F.2.

4.3 Tree-prompted LLM Inference

Motivation: Based on the structural encoding tree \mathcal{T} , we further integrate node language descriptions to enable comprehensive in-context learning with LLMs, fostering a better understanding of both topology and textual information in the original graph. This allows LLMs to make reliable inferences without fine-tuning. These inferences are then used to optimize the encoding tree, enhancing homophily within low-level communities and laying a strong foundation for subsequent GSL.

Reception-aware Leaf Augmentation. To construct effective in-context prompts for LLMs, the quality of node-specific text is essential. Thus, we perform tree-guided text propagation and aggregation within each low-level community $\mathcal{C}^\ell(i)$ to achieve leaf augmentation for ϵ -guaranteed t^* . The key idea is that nodes in low-level communities typically show high connectivity and homophily, enabling efficient text sharing. Using this property, we filter and combine relevant texts for each leaf node based on a similarity threshold ϵ , helping to reduce noise. This process is formally defined as:

$$t_\alpha^* = \text{Concat}(\{t_\alpha\} \cup \{t_j \mid j \in \text{Top}_k(\{w_{\alpha\beta} \mid \beta \in \mathcal{C}^\ell(\alpha)\}), w_{\alpha\beta} \geq \epsilon\}), \quad (2)$$

$$w_{\alpha\beta} = \frac{\exp(\text{sim}(x_\alpha, x_\beta))}{\sum_{\gamma \in \mathcal{C}^\ell(\alpha)} \exp(\text{sim}(x_\alpha, x_\gamma))}, \quad \text{sim}(x_\alpha, x_\beta) = \frac{\sum_{i=1}^{f\text{-dim}} x_\alpha^i \cdot x_\beta^i}{\sqrt{\sum_{i=1}^{f\text{-dim}} (x_\alpha^i)^2 \sum_{i=1}^{f\text{-dim}} (x_\beta^i)^2}}. \quad (3)$$

Community of Thought. Leveraging the enhanced leaf nodes, we propose a community of thought (CoT) prompt mechanism, which contains the community-enhanced descriptions for each node and its community-related neighbors for more reliable LLM inference. Based on this, we enable the LLM to fully understand both the topology and text insights of the original graph, accurately infer the probabilities of a node belonging to each label class, and generate high-quality embeddings within the LLM’s semantic encoding space by softmax. These embedding are subsequently used for fine-grained tree optimization. In a nutshell, this approach facilitates efficient LLM in-context learning through the structural encoding tree-driven CoT. The above inference and encoding process can be formally defined as:

$$z_\alpha = \text{Extract}(\text{ANS}_\alpha), \quad \text{ANS}_\alpha = \text{LLM-CoT}(\mathcal{D}_{task}, \mathcal{D}_{topo}, \mathcal{D}_{sema}, t_\alpha^*), \quad (4)$$

$$y_\alpha^{cls} = \text{Softmax}(z_\alpha) \text{ if } (|z| = N_{class}) \text{ and } (\forall i \in \{1, \dots, N_{class}\}, 0 \leq z_i \leq 9), \quad (5)$$

where $\text{Extract}(\cdot)$ is the operation for extracting the list of label class probabilities. \mathcal{D}_{task} is the task description. \mathcal{D}_{topo} and \mathcal{D}_{sema} represent the descriptions of topological and semantic information, respectively. $[\text{ANS}]$ is the inference result of LLM and $y_\alpha^{cls} \in \mathbf{Y}^{cls}$ is the soft label for each leaf node. For the prompt construction example, we refer the reader to Fig. 2.

Theorem 3 (Error Bound Between Soft labels and True Labels). *Given two leaf nodes α and β in \mathcal{T} , the error between soft label similarity and true label similarity is bounded by:*

$$\varepsilon^y(\alpha\beta) = |\text{sim}(y_\alpha^{cls}, y_\beta^{cls}) - \text{sim}(y_\alpha, y_\beta)| \leq \delta \cdot (1 - \epsilon), \text{ where } \delta \text{ is a constant that depends on the LLM’s in-context learning ability and } y_\alpha \text{ is the true label of } \alpha. \text{ (The proof is detailed in Appendix F.3.)}$$

Based on Theorem 3, we have that the similarity of soft labels y^{cls} can approximate the similarity of ground-truth labels y with controllable bias $\varepsilon^y(\alpha\beta)$. This provides robust theoretical guarantee and support for the subsequent **Leaf Dependency Allocation** and **Semantic Similarity Sampling**.

Leaf Dependency Allocation. Although the structural encoding tree captures the topology of the original graph, another critical factor is the text-driven node attributes. Therefore, we optimize the low-level communities by reallocating leaf dependencies, guided by soft labels from the LLM, thus enhancing GSL with text insights. To achieve this, we first initialize the leaf-community clusters based on the original structural encoding tree. Next, we apply adaptive clustering using the silhouette coefficient to refine community assignments. The main goal is to enhance homophily within low-level communities, ensuring that most nodes in each cluster share the same label. Specifically, (1) we reallocate leaf nodes with minority labels to align with the dominant class in each community, and (2) we adaptively increase the number of clusters by leveraging the silhouette coefficient, allowing the formation of new communities that better capture homophily. An illustrative example is shown in Fig.2. This process yields the optimized structural encoding tree \mathcal{T}^* , which serves as the foundation for defining the tree sampler. The adaptive clustering algorithm is detailed in Appendix E.2.

4.4 Leaf-oriented Two-step Sampling

Motivation. Although structural optimization can be applied to all leaf nodes, we adopt a two-step sampling technology to balance running efficiency and practical performance. Specifically, we first identify a limited set of nodes requiring optimization from a topological perspective. Subsequently, we select a candidate set of nodes closely related to these nodes from a text semantic perspective. Finally, through edge addition or removal, we facilitate training-free GSL. The detailed algorithm of the two-step sampling can be found in Appendix E.3.

Theorem 4 (High-Entropy Nodes Require Supervision). *In a structural encoding tree \mathcal{T} constructed via entropy minimization, nodes with higher structural entropy $\mathcal{H}^T(\mathcal{G}, \alpha)$ indicate: higher topological uncertainty within their local structural context. (The proof is detailed in Appendix F.4.)*

Topology Uncertainty Sampling. As we all know, the core of GSL is to eliminate graph structural noise to enhance data utility. Notably, this noise typically does not pervade the entire graph but exists in certain graph substructures. According to Theorem 4, nodes with higher structural entropy are more likely to reside in topologically uncertain regions and thus benefit more from supervision-aware structural refinement. Therefore, to improve running efficiency, we leverage structural entropy to quantify the priority of nodes in need of structural optimization. Specifically, within each leaf community $\mathcal{C}^\ell(i)$, we use structural entropy $\mathcal{H}^T(\mathcal{G}, \alpha)$ to assign probabilities to each leaf node for node-wise sampling:

$$\mathcal{P}_{topo}(\alpha) = \frac{\exp(\mathcal{H}^T(\mathcal{G}, \alpha))}{\sum_{\gamma \in \mathcal{C}^\ell(\alpha)} \exp(\mathcal{H}^T(\mathcal{G}, \gamma))}. \quad (6)$$

Semantic Similarity Sampling. To ensure practical performance, we filter the remaining leaf nodes (excluding α) by LLM-empowered semantic similarity y^{cls} to obtain a θ -sized candidate set. The node β in this candidate set is utilized for edge addition or removal with α . For edge addition, the sampling probabilities are ranked in descending order of similarity, while for edge removal, they are ranked in ascending order. The above edge-wise sampling is defined as:

$$\mathcal{P}_{sema}^\alpha(\beta) = \frac{\exp(\text{sim}(y_\beta^{cls}, y_\alpha^{cls}))}{\sum_{\gamma \in \mathcal{C}^\ell(\alpha), \gamma \neq \alpha} \exp(\text{sim}(y_\gamma^{cls}, y_\alpha^{cls}))}. \quad (7)$$

5 Experiment

In this section, we conduct a wide range of experiments and aim to answer: **Q1: Effectiveness.** Compared with other state-of-the-art GSL methods, can LLaTA achieve better performance? **Q2: Interpretability.** If LLaTA is effective, what contributes to its outstanding performance? **Q3: Robustness.** How does LLaTA perform when deployed in real-world complex scenarios? **Q4: Efficiency.** How efficient is LLaTA compared to other competitive GSL methods?

5.1 Experiment Setup

We evaluate LLaTA and 13 GSL baselines on 10 widely adopted TAG datasets across multiple domains. The details on these datasets and baselines can be found in Appendix G-H. Due to space limitations, the hyperparameter settings used in the experiments are provided in the Appendix I.

5.2 Performance Comparison

Node Classification. To answer **Q1**, we first present the node classification performance results in Table 1, where LLaTA consistently outperforms other baselines. For instance, LLaTA outperforms the second-best method by 1.18%, 1.02%, and 1.07% on the Cora, WikiCS, and Instagram datasets, respectively. Moreover, LLaTA demonstrates significant gains in complex History and Photo, outperforming the second-best methods by 2.45% and 2.78%. Notably, on the Child dataset, LLaTA achieves an impressive improvement of 9.87%, highlighting its strong capability in handling heterophily. These results underscore LLaTA’s effectiveness in achieving superior performance.

Node Clustering. To further answer **Q1**, we conducted a comprehensive comparison of LLaTA with GSL methods that have demonstrated strong performance in node classification, extending to node clustering. As shown in Table 2, LLaTA consistently outperforms competing methods across all four datasets, significantly enhancing the effectiveness of GNNs in unsupervised tasks. These results confirm that LLaTA is applicable to diverse tasks, demonstrating its generalization and adaptability.

5.3 Ablation Study

To answer **Q2**, we conduct an ablation study shown in Table 3 and provide a case study in Appendix J, which provides a detailed analysis of our method’s pipeline by visualizing the data flow. Meanwhile, we provide LLM backbone analysis

Table 1: Node classification accuracy(%) on 10 TAG datasets. Shown is the *mean* \pm *std* of 10 runs with different random seeds. Highlighted are the top **first**, **second**, and **third** accuracy. OOM denotes out of memory and OOT denotes time limits of 72 hours exceeded.

Method	Cora	Citeseer	Pubmed	WikiCS	Instagram	Reddit	Ratings	Child	History	Photo
IDGL	86.81 \pm 0.31	75.39 \pm 0.27	87.25 \pm 0.22	79.78 \pm 0.14	63.68 \pm 0.09	65.03\pm0.13	44.01\pm0.29	45.33 \pm 0.26	80.46 \pm 0.31	82.33\pm0.33
SLAPS	79.89 \pm 0.50	73.51 \pm 0.64	86.41 \pm 0.49	72.50 \pm 0.27	60.91 \pm 0.13	OOM	40.76 \pm 0.23	47.46 \pm 0.21	OOM	OOM
GAUGO	85.24 \pm 0.27	75.24 \pm 0.43	87.12 \pm 0.38	70.74 \pm 0.29	63.34 \pm 0.21	OOM	40.19 \pm 0.24	47.27 \pm 0.19	OOM	OOM
HESGSL	85.91 \pm 0.45	76.03 \pm 0.31	87.17 \pm 0.27	73.29 \pm 0.22	63.83 \pm 0.16	OOM	38.71 \pm 0.42	47.81 \pm 0.25	OOM	OOM
SEGL	86.90\pm0.54	76.52\pm0.20	87.42 \pm 0.38	79.68 \pm 0.29	65.26\pm0.21	64.87 \pm 0.26	43.20 \pm 0.47	51.80\pm0.39	OOT	OOT
ProGNN	84.18 \pm 0.23	75.08 \pm 0.21	86.89 \pm 0.14	71.90 \pm 0.16	64.45 \pm 0.19	OOM	OOM	OOM	OOM	OOM
SUBLIME	84.81 \pm 0.33	75.55 \pm 0.47	87.63\pm0.70	78.06 \pm 0.38	64.78 \pm 0.24	58.82 \pm 0.21	39.90 \pm 0.17	49.54 \pm 0.16	OOM	OOM
STABLE	84.21 \pm 0.43	75.34 \pm 0.60	87.27 \pm 0.39	76.93 \pm 0.33	65.66\pm0.18	59.78 \pm 0.24	40.55 \pm 0.10	50.90 \pm 0.09	OOM	OOM
CoGSL	86.16 \pm 0.45	75.45 \pm 0.36	OOM							
BORF	87.08\pm0.18	76.43 \pm 0.17	87.45\pm0.11	80.56\pm0.08	64.07 \pm 0.06	63.07 \pm 0.09	42.72 \pm 0.60	50.92 \pm 0.54	82.83\pm0.14	82.63\pm0.15
DHGR	86.72 \pm 0.42	76.18 \pm 0.14	86.76 \pm 0.33	79.25 \pm 0.17	64.26 \pm 0.26	66.41\pm0.29	43.33\pm0.36	52.41\pm0.40	82.61\pm0.16	81.92 \pm 0.18
GraphEdit	86.26 \pm 1.06	76.33 \pm 1.12	87.14 \pm 0.29	79.92\pm0.63	64.23 \pm 1.01	OOT	OOT	OOT	OOT	OOT
LLM4RGNN	86.73 \pm 0.73	76.96\pm0.58	87.37 \pm 0.21	OOT						
LLaTA (Ours)	88.26\pm0.26	78.21\pm0.18	88.39\pm0.23	81.58\pm0.20	66.73\pm0.13	67.60\pm0.19	44.47\pm0.08	62.28\pm0.56	85.28\pm0.24	85.41\pm0.24

Table 2: Comparison of node clustering.

Method	Cora	Citeseer	Pubmed	Instagram
GCN	66.42 \pm 0.16	70.28 \pm 0.14	78.95 \pm 0.07	64.59 \pm 0.01
SEGL	67.70 \pm 0.17	71.15 \pm 0.12	79.05 \pm 0.04	64.63 \pm 0.01
BORF	67.54 \pm 0.16	70.62 \pm 0.10	79.46 \pm 0.03	64.49 \pm 0.02
DHGR	66.85 \pm 0.63	70.14 \pm 0.21	78.64 \pm 0.15	64.52 \pm 0.06
LLM4RGNN	67.63 \pm 0.11	71.72 \pm 0.13	78.90 \pm 0.06	OOT
LLaTA	68.39\pm0.14	72.18\pm0.15	80.25\pm0.06	65.37\pm0.02

Table 3: Ablation study result of LLaTA.

Component	Pubmed	WikiCS	Instagram	Ratings
w/o TO	85.34 \pm 0.35	78.63 \pm 0.28	64.06 \pm 0.23	42.05 \pm 0.14
w/o TO _{LLM}	86.81 \pm 0.26	80.03 \pm 0.22	64.94 \pm 0.15	42.87 \pm 0.11
w/o Sam _{LLM}	86.68 \pm 0.30	80.23 \pm 0.25	64.81 \pm 0.18	42.72 \pm 0.13
w/ LLM _{NE}	87.04 \pm 0.21	80.09 \pm 0.20	65.13 \pm 0.14	41.96 \pm 0.09
w/ LLM _{RW}	87.23 \pm 0.21	80.46 \pm 0.19	65.57 \pm 0.15	42.40 \pm 0.11
LLaTA	88.39\pm0.23	81.58\pm0.20	66.73\pm0.13	44.47\pm0.08

in Appendix K. In the ablation study, we use TO to denote tree optimization, while TO_{LLM} and Sam_{LLM} denote the tree optimization and sampling processes with LLM. For the ablation setup, the LLM inference results are replaced by the initial features. Additionally, LLM_{NE} and LLM_{RW} represent LLM inference with topology-aware tree in-context information derived from 1-hop neighbors and random walk sequences, rather than the tree, respectively.

From the ablation study, we obtain the following key conclusions: (1) Removing TO leads to a significant performance decline, indicating that the tree plays a crucial role in LLM-based GSL. (2) Replacing LLM inference results with initial node features to guide TO and Sam leads to a performance decline. This highlights the critical role of LLM-generated contextual information, as initial node features alone are inadequate for capturing complex semantic relationships. (3) Utilizing 1-hop neighbors and random walk sequences to provide topology-aware in-context information also results in performance degradation. This highlights the necessity of the SE-based hierarchical structural encoding tree. Meanwhile, SE provides valuable guidance for node sampling, a capability that cannot be effectively achieved solely with 1-hop neighbors or random walk sequences.

5.4 Robustness Analysis

To answer Q3, we conduct a thorough analysis of the LLaTA’s robustness from the following aspects:

Downstream Backbones. According to Table 4, LLaTA consistently outperforms the base models across all datasets, achieving notable improvements of up to 10.18% for GCN and 9.31% for GAT. Although the gains for GraphSAGE are smaller, this can be attributed to its strong inherent node representation capability. Overall, these results demonstrate LLaTA’s robustness in enhancing various GNN backbones, highlighting its broad applicability across mainstream architectures.

Real-world Scenarios. To evaluate the robustness of LLaTA against sparsity and noise scenarios in practical applications, we randomly remove or add edges to the original graph structure. As illustrated in Fig. 3, LLaTA demonstrates strong predictive performance in both scenarios. In the sparse setting, LLaTA achieves optimal performance across most perturbation levels. In the noisy scenario, LLaTA performs competitively, with only LLM4RGNN surpassing it, as the latter is specifically designed to handle graph adversarial attack settings. Notably, as the edge addition rate increases, the performance of LLaTA gradually deteriorates, which can be attributed to the irreversible negative impact of such perturbations on the tree initialization.

Hyperparameter. We conducted a comprehensive analysis of the four key hyperparameters of LLaTA: K , ϵ , θ , and r . The experimental results for K , θ , and r are presented in Fig. 4, while the analysis of ϵ and the experimental results of θ , r on other datasets are provided in Appendix L. In Fig. 4 (left), we see that the optimal encoding tree height K varies by dataset, with $K = 3$ for WikiCS and Pubmed, and $K = 2$ for Instagram. However, when K increases to 5, performance significantly drops across all datasets, suggesting that excessive tree depth may cause overfitting or loss of

Table 4: Improvements (compare to GNN) of LLaTA with different GNN backbones.

Dataset	LLaTA _{GCN}	LLaTA _{GAT}	LLaTA _{SAGE}
Reddit	67.60 \pm 0.11	63.80 \pm 0.13	60.73 \pm 0.13
Child	62.28 \pm 0.12	62.65 \pm 0.12	63.53 \pm 0.14
History	85.28 \pm 0.12	85.30 \pm 0.12	84.67 \pm 0.11
Photo	85.41 \pm 0.13	85.38 \pm 0.12	82.20 \pm 0.12
Improvement	\uparrow 1.79~10.18	\uparrow 1.38~9.31	\uparrow 0.56~9.35

Table 5: Time complexity analysis of LLaTA and other GSL method.

Method	Time complexity
SEGSL	$\mathcal{O}(n^2 + n \log^2 n + n)$
GraphEdit LLM4RGNN	$\mathcal{O}(pt_{\text{LLM-f}} + qd^2 + n^2 + (m + nk)t_{\text{LLM-i}})$ $\mathcal{O}(pt_{\text{LLM-f}} + mt_{\text{LLM-i}} + qd^2 + n^2)$
LLaTA	$\mathcal{O}(n \log^2 n + n \mathcal{C} ^2 + nt_{\text{LLM-i}} + n)$

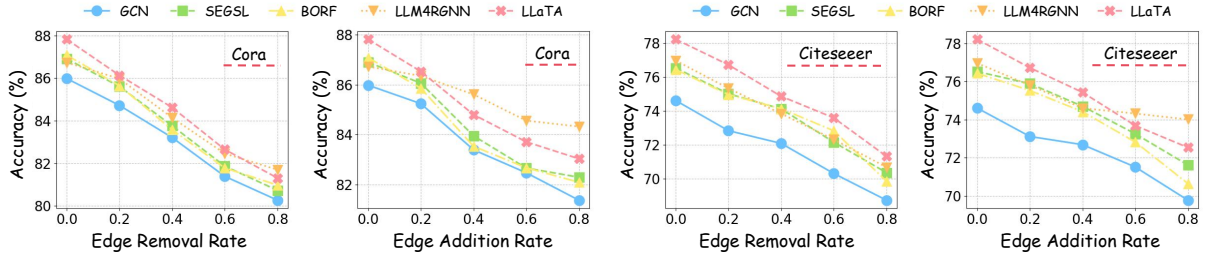


Figure 3: Node classification performance on the Cora and Citeseer dataset under real-world scenarios (sparse [Edge Removal] and noise [Edge Addition]).

structural information. In Fig. 4 (right), we analyze LLaTA’s sensitivity to the candidate set size θ in semantic similarity sampling and the two-step sampling frequency r on the Cora dataset. The results indicate that an r value between 3 and 10 yields higher accuracy, corresponding to an appropriately improved graph density. In contrast, LLaTA is less sensitive to the choice of θ , achieving stable performance within the range of $\theta \in [5, 15]$. A smaller θ may result in insufficient semantic similarity sampling, whereas a larger θ could introduce noise into the candidate set, negatively impacting performance.

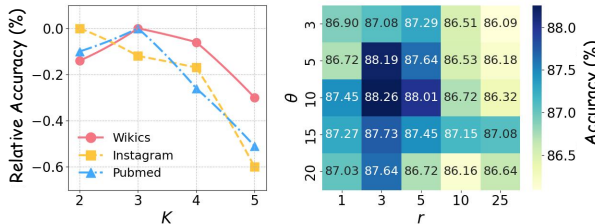
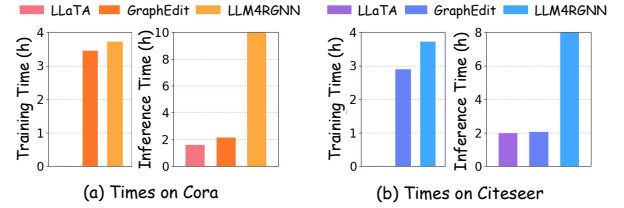
Figure 4: Hyperparameter analysis of K , θ and r . θ and r are analyzed on the Cora dataset.

Figure 5: Comparison of training and inference time for LLM-based GSL method.

5.5 Efficiency analysis

To answer **Q4**, we conduct a theoretical analysis of the algorithm time complexity of LLaTA and empirically demonstrate its efficiency in integrating LLMs with GSL.

In Table 5, we analyze the theoretical time complexity of LLaTA and existing LLM-based GSL methods. Where q and p is the number of samples for fine-tuning and edge predictor training, respectively. $t_{\text{LLM-f}}$ and $t_{\text{LLM-i}}$ denote the fine-tuning and inference time of LLM, respectively. The magnitude of $t_{\text{LLM-i}}$ should be adaptively determined according to the specific requirements of different inference tasks. For LLaTA, The time complexity can be divided into three parts: (a) The complexity for tree construction in Sec. 4.2 is $\mathcal{O}(n \log^2 n)$, (b) The complexity of tree-prompted LLM inference in Sec. 4.3 is $\mathcal{O}(n|\mathcal{C}|^2 + nt_{\text{LLM-i}})$, (c) The complexity of the two-step sampling in Sec. 4.4 is $\mathcal{O}(\theta n)$. Complete runtime results of LLaTA across all datasets are provided Appendix M.

To practically evaluate the efficiency of LLaTA, we compare its training and inference time with existing all LLM-based GSL methods. The training time includes the fine-tuning process of the LLM and the training of the edge predictor, while the inference time encompasses LLM inference and other GSL modules. As shown in Fig. 5, the experimental results demonstrate that our method requires significantly less inference time, particularly when compared to LLM4RGNN. Furthermore, our approach eliminates the need for any training during the structure learning phase, resulting in zero training time. This highlights the efficiency of our method in seamlessly integrating LLMs with GSL.

6 Conclusion

In this paper, we first introduce a novel optimization framework for GSL by rethinking its integration with LLMs, addressing the challenges of incorporating textual information. Subsequently, We propose LLaTA as an instantiation of this novel framework, which leverages a structural encoding tree to achieve efficient LLM in-context learning. This enables the LLM to comprehensively understand both topology and text insights from the original graph, ultimately relying on reliable inference to obtain improved graph structure. To this end, LLaTA eliminates the need for costly fine-tuning and achieves SOTA performance. Inspired by the noise experiments, a promising direction is developing more robust tree optimization algorithms, laying a solid foundation for LLM-empowered GSL.

References

- [1] Wendong Bi, Lun Du, Qiang Fu, Yanlin Wang, Shi Han, and Dongmei Zhang. Make heterophilic graphs better fit gnn: A graph rewiring approach. *IEEE Transactions on Knowledge and Data Engineering*, 2024.
- [2] Yu Chen, Lingfei Wu, and Mohammed Zaki. Iterative deep graph learning for graph neural networks: Better and robust node embeddings. *Advances in neural information processing systems*, 33:19314–19326, 2020.
- [3] Zhikai Chen, Haitao Mao, Jingzhe Liu, Yu Song, Bingheng Li, Wei Jin, Bahare Fatemi, Anton Tsitsulin, Bryan Perozzi, Hui Liu, et al. Text-space graph foundation models: Comprehensive benchmarks and new insights. *arXiv preprint arXiv:2406.10727*, 2024.
- [4] Enyan Dai, Shijie Zhou, Zhimeng Guo, and Suhang Wang. Label-wise graph convolutional network for heterophilic graphs. In *Learning on Graphs Conference, LoG*, pages 26–1. PMLR, 2022.
- [5] Lun Du, Xiaozhou Shi, Qiang Fu, Xiaojun Ma, Hengyu Liu, Shi Han, and Dongmei Zhang. Gbk-gnn: Gated bi-kernel graph neural networks for modeling both homophily and heterophily. In *Proceedings of the ACM Web Conference, WWW*, pages 1550–1558, 2022.
- [6] Bahare Fatemi, Layla El Asri, and Seyed Mehran Kazemi. Slaps: Self-supervision improves structure learning for graph neural networks. *Advances in Neural Information Processing Systems*, 34:22667–22681, 2021.
- [7] Zirui Guo, Lianghao Xia, Yanhua Yu, Yuling Wang, Zixuan Yang, Wei Wei, Liang Pang, Tat-Seng Chua, and Chao Huang. Graphedit: Large language models for graph structure learning. *arXiv preprint arXiv:2402.15183*, 2024.
- [8] Will Hamilton, Zhitao Ying, and Jure Leskovec. Inductive representation learning on large graphs. *Advances in neural information processing systems*, 30, 2017.
- [9] Xuanwen Huang, Kaiqiao Han, Yang Yang, Dezheng Bao, Quanjin Tao, Ziwei Chai, and Qi Zhu. Can gnn be good adapter for llms? In *Proceedings of the ACM on Web Conference 2024*, pages 893–904, 2024.
- [10] Xinke Jiang, Zidi Qin, Jiarong Xu, and Xiang Ao. Incomplete graph learning via attribute-structure decoupled variational auto-encoder. In *Proceedings of the 17th ACM International Conference on Web Search and Data Mining*, pages 304–312, 2024.
- [11] Wei Jin, Yao Ma, Xiaorui Liu, Xianfeng Tang, Suhang Wang, and Jiliang Tang. Graph structure learning for robust graph neural networks. In *Proceedings of the 26th ACM SIGKDD international conference on knowledge discovery & data mining*, pages 66–74, 2020.
- [12] Thomas N Kipf and Max Welling. Semi-supervised classification with graph convolutional networks. *arXiv preprint arXiv:1609.02907*, 2016.
- [13] Angsheng Li and Yicheng Pan. Structural information and dynamical complexity of networks. *IEEE Transactions on Information Theory*, 62(6):3290–3339, 2016.
- [14] Kuan Li, Yang Liu, Xiang Ao, Jianfeng Chi, Jinghua Feng, Hao Yang, and Qing He. Reliable representations make a stronger defender: Unsupervised structure refinement for robust gnn. In *Proceedings of the 28th ACM SIGKDD conference on knowledge discovery and data mining*, pages 925–935, 2022.
- [15] Xunkai Li, Zhengyu Wu, Jiayi Wu, Hanwen Cui, Jishuo Jia, Rong-Hua Li, and Guoren Wang. Graph learning in the era of llms: A survey from the perspective of data, models, and tasks. *arXiv preprint arXiv:2412.12456*, 2024.
- [16] Nian Liu, Xiao Wang, Lingfei Wu, Yu Chen, Xiaojie Guo, and Chuan Shi. Compact graph structure learning via mutual information compression. In *Proceedings of the ACM web conference 2022*, pages 1601–1610, 2022.
- [17] Yiwei Liu, Jiamou Liu, Zijian Zhang, Liehuang Zhu, and Angsheng Li. Rem: From structural entropy to community structure deception. *Advances in Neural Information Processing Systems*, 32, 2019.
- [18] Yixin Liu, Yu Zheng, Daokun Zhang, Hongxu Chen, Hao Peng, and Shirui Pan. Towards unsupervised deep graph structure learning. In *Proceedings of the ACM Web Conference 2022*, pages 1392–1403, 2022.
- [19] Dongsheng Luo, Wei Cheng, Wenchao Yu, Bo Zong, Jingchao Ni, Haifeng Chen, and Xiang Zhang. Learning to drop: Robust graph neural network via topological denoising. In *Proceedings of the 14th ACM international conference on web search and data mining*, pages 779–787, 2021.
- [20] Péter Mernyei and Cătălina Cangea. Wiki-cs: A wikipedia-based benchmark for graph neural networks. *arXiv preprint arXiv:2007.02901*, 2020.
- [21] Khang Nguyen, Nong Minh Hieu, Vinh Duc Nguyen, Nhat Ho, Stanley Osher, and Tan Minh Nguyen. Revisiting over-smoothing and over-squashing using ollivier-ricci curvature. In *International Conference on Machine Learning*, pages 25956–25979. PMLR, 2023.

- [22] Yicheng Pan, Feng Zheng, and Bingchen Fan. An information-theoretic perspective of hierarchical clustering. *arXiv preprint arXiv:2108.06036*, 2021.
- [23] Claude Elwood Shannon. A mathematical theory of communication. *The Bell system technical journal*, 27(3):379–423, 1948.
- [24] Yunchong Song, Chenghu Zhou, Xinbing Wang, and Zhouhan Lin. Ordered gnn: Ordering message passing to deal with heterophily and over-smoothing. *International conference on learning representations, ICLR*, 2023.
- [25] Ashish Vaswani, Noam Shazeer, Niki Parmar, Jakob Uszkoreit, Llion Jones, Aidan N Gomez, Łukasz Kaiser, and Illia Polosukhin. Attention is all you need. *Advances in neural information processing systems*, 30, 2017.
- [26] Petar Veličković, Guillem Cucurull, Arantxa Casanova, Adriana Romero, Pietro Lio, and Yoshua Bengio. Graph attention networks. *arXiv preprint arXiv:1710.10903*, 2017.
- [27] Junran Wu, Xueyuan Chen, Ke Xu, and Shangzhe Li. Structural entropy guided graph hierarchical pooling. In *International conference on machine learning*, pages 24017–24030. PMLR, 2022.
- [28] Lirong Wu, Haitao Lin, Zihan Liu, Zicheng Liu, Yufei Huang, and Stan Z Li. Homophily-enhanced self-supervision for graph structure learning: Insights and directions. *IEEE Transactions on Neural Networks and Learning Systems*, 2023.
- [29] Hao Yan, Chaozhuo Li, Ruosong Long, Chao Yan, Jianan Zhao, Wenwen Zhuang, Jun Yin, Peiyan Zhang, Weihao Han, Hao Sun, et al. A comprehensive study on text-attributed graphs: Benchmarking and rethinking. *Advances in Neural Information Processing Systems*, 36:17238–17264, 2023.
- [30] Zhenyu Yang, Ge Zhang, Jia Wu, Jian Yang, Quan Z Sheng, Hao Peng, Angsheng Li, Shan Xue, and Jianlin Su. Minimum entropy principle guided graph neural networks. In *Proceedings of the sixteenth ACM international conference on web search and data mining*, pages 114–122, 2023.
- [31] Zhongjian Zhang, Xiao Wang, Huichi Zhou, Yue Yu, Mengmei Zhang, Cheng Yang, and Chuan Shi. Can large language models improve the adversarial robustness of graph neural networks? *arXiv preprint arXiv:2408.08685*, 2024.
- [32] Tong Zhao, Yozen Liu, Leonardo Neves, Oliver Woodford, Meng Jiang, and Neil Shah. Data augmentation for graph neural networks. In *Proceedings of the aaai conference on artificial intelligence*, volume 35, pages 11015–11023, 2021.
- [33] Cheng Zheng, Bo Zong, Wei Cheng, Dongjin Song, Jingchao Ni, Wenchao Yu, Haifeng Chen, and Wei Wang. Robust graph representation learning via neural sparsification. In *International Conference on Machine Learning*, pages 11458–11468. PMLR, 2020.
- [34] Yilun Zheng, Zhuofan Zhang, Ziming Wang, Xiang Li, Sitao Luan, Xiaojiang Peng, and Lihui Chen. Rethinking structure learning for graph neural networks. *arXiv preprint arXiv:2411.07672*, 2024.
- [35] Zhou Zhiyao, Sheng Zhou, Bochao Mao, Xuanyi Zhou, Jiawei Chen, Qiaoyu Tan, Daochen Zha, Yan Feng, Chun Chen, and Can Wang. Opengsl: A comprehensive benchmark for graph structure learning. *Advances in Neural Information Processing Systems*, 36, 2024.
- [36] Yanqiao Zhu, Weizhi Xu, Jinghao Zhang, Qiang Liu, Shu Wu, and Liang Wang. Deep graph structure learning for robust representations: A survey. *arXiv preprint arXiv:2103.03036*, 14:1–1, 2021.
- [37] Dongcheng Zou, Hao Peng, Xiang Huang, Renyu Yang, Jianxin Li, Jia Wu, Chunyang Liu, and Philip S Yu. Se-gsl: A general and effective graph structure learning framework through structural entropy optimization. In *Proceedings of the ACM Web Conference 2023*, pages 499–510, 2023.

A Encoding Tree and Structural Entropy

In this section, we provide a detailed exposition of the formal definitions of the encoding tree and related structural entropy. Based on this, we present a visualized toy example in Fig. 6 to intuitively illustrate the practical significance of leaf nodes, low-level communities, and higher-level communities, offering readers a clearer conceptual understanding.

Definition 1. Encoding Tree. *The language-aware encoding tree \mathcal{T} of a node-wise TAG $\mathcal{G} = (\mathcal{V}, \mathcal{E}, \mathbb{T})$ satisfies the following properties:*

- (1) *The root node λ has a partition (community) $\mathcal{P}_\lambda^{tree} = \mathcal{V}$, where \mathcal{V} represents the set of all vertices in \mathcal{G} .*
- (2) *Each non-root node α has a partition $\mathcal{P}_\alpha^{tree} \subset \mathcal{V}$. If α is a leaf node, $\mathcal{P}_\alpha^{tree}$ is a singleton with one vertex from \mathcal{V} .*
- (3) *For each leaf node α with $\mathcal{P}_\alpha^{tree} = v_i$, $x_\alpha = x_i$ is the initial embedding of α , and $t_\alpha = t_i$ is the raw text of α .*
- (4) *For each non-root node α , the parent node of the community to which it belongs is denoted as α^+ .*
- (5) *Each non-leaf node α , its i -th child node is denoted as $\alpha^{(i)}$, where the children are ordered from left to right as i increases. If α is not λ , it can be considered as a community.*
- (6) *For each non-leaf node α , assuming it has m children, the partitions of its children $\mathcal{P}_{\alpha^{(i)}}^{tree}$ together form the partition of $\mathcal{P}_\alpha^{tree}$, so that $\mathcal{P}_\alpha^{tree} = \bigcup_{i=1}^m \mathcal{P}_{\alpha^{(i)}}^{tree}$ and $\bigcap_{i=1}^m \mathcal{P}_{\alpha^{(i)}}^{tree} = \emptyset$. If the height of the encoding tree is restricted to K , it is called a K -level encoding tree.*

Definition 2. Structural Entropy. *Based on the above definition, structural entropy can be used to quantify the dynamic complexity of such hierarchical trees, revealing their inherent topology insights. For the K -height encoding tree \mathcal{T} , the K -dimensional structural entropy of \mathcal{G} is defined as:*

$$\mathcal{H}^K(\mathcal{G}) = \min_{\forall \mathcal{T}: \text{height}(\mathcal{T}) \leq K} \{\mathcal{H}^{\mathcal{T}}(\mathcal{G})\} \quad (8)$$

$$\mathcal{H}^{\mathcal{T}}(\mathcal{G}) = \sum_{\alpha \in \mathcal{T}, \alpha \neq \lambda} \mathcal{H}^{\mathcal{T}}(\mathcal{G}, \alpha) = - \sum_{\alpha \in \mathcal{T}, \alpha \neq \lambda} \frac{g_\alpha}{\text{vol}(\mathcal{G})} \log_2 \frac{\text{vol}(\alpha)}{\text{vol}(\alpha^+)} \quad (9)$$

where g_α represents the sum of the weights of cross-node edges that connect nodes within partition $\mathcal{P}_\alpha^{tree}$ to nodes outside $\mathcal{P}_\alpha^{tree}$. $\text{vol}(\alpha)$ denotes the sum of the degrees of all nodes within $\mathcal{P}_\alpha^{tree}$. $\mathcal{H}^{\mathcal{T}}(\mathcal{G}, \alpha)$ is the structural entropy of node α , representing the K -dimensional structural entropy of α when the height of \mathcal{T} is K . The core of this measurement lies in the observation that, in a highly connected graph, nodes frequently interact with their neighbors. By employing random walks, these interactions can be captured, and entropy can be introduced as a measure of topology uncertainty [13]. Specifically, the one-dimensional structural measurement of \mathcal{G} can be quantified using the stationary distribution of its degrees d and Shannon entropy. This concept can be generalized to K -dimensional measurements using the structural encoding tree in Definition 1.

B Analysis of Hierarchical Community

In the encoding tree, the communities of leaf nodes are referred to as low-level communities, which are directly instantiated through the parent nodes of the leaf nodes. In contrast, communities at higher levels are referred to as higher-level communities. Low-level communities primarily capture local topological structures, often exhibiting homophily (i.e., connected nodes are more likely to share similar feature distributions or the same labels.) in TAGs, and represent local clusters or groups within the graph. These communities typically include strongly interrelated nodes, such as teams or social groups. Higher-level communities, on the other hand, are more abstract and loosely connected, formed by aggregating multiple low-level communities. They reveal high-level structural patterns or inter-community relationships, focus more on capturing global topological structures.

In Fig. 6, we present a toy example illustrating hierarchical semantics in a social network. It represents student social interactions, where nodes correspond to individual students, and edges denote relationships between them. Nodes of the same color represent students belonging to the same class (C-1, C-2, C-3), while red and blue nodes represent students sharing the same major (M-1), and green nodes represent students from a different major (M-2). The structural encoding tree reveals that low-level communities correspond to tightly connected classmates, while higher-level communities represent majors encompassing multiple classes. Although connections exist from different classes, they are less cohesive than those within the same class.

In LLaTA, we focus on low-level communities as they capture local relationships between nodes, which are critical for specific downstream tasks. Specifically, these communities reveal clearer and more concrete structural patterns, making them directly applicable to enhance GSL. In contrast, higher-level communities often represent latent high-level

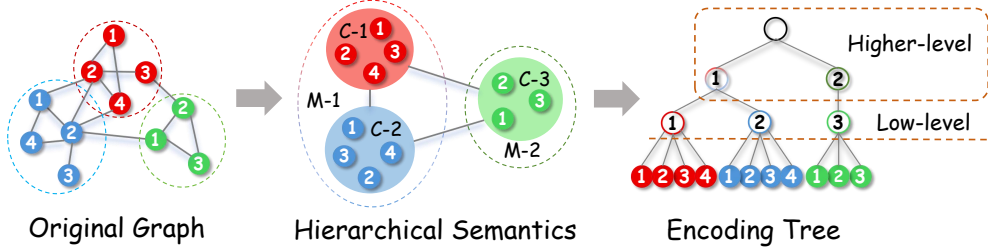


Figure 6: An illustrative example of hierarchical communities (semantics) in a simple social network.

structural patterns, which is unclear and unintuitive. This makes them not well-suited for direct application in GSL. Furthermore, unlike naive neighborhood-based clusters, bottom-level communities capture local structural patterns while being shaped by global structural constraints.

While low-level communities are primarily focused on capturing local topological structure, they are not simple local neighborhoods. Under the global structural entropy minimization principle [13], the construction of the encoding tree ensures that each module, including those at the bottom level, is formed in a way that minimizes global uncertainty and boundary complexity.

From the random walk perspective, the structural entropy $\mathcal{H}^T(\mathcal{G})$ quantifies the average uncertainty of a walker’s position in the network under a hierarchical modular encoding. As shown in [13], the structural entropy with respect to a flat partition \mathcal{P} can be decomposed as:

$$\mathcal{H}^{\mathcal{P}}(\mathcal{G}) = \sum_{\alpha \in \mathcal{T}} \frac{\text{vol}(\alpha)}{\text{vol}(\mathcal{G})} \cdot H \left(\left\{ \frac{d_i^{(\alpha)}}{\text{vol}(\alpha)} \right\}_{i=1}^{n_\alpha} \right) - \sum_{\alpha \in \mathcal{T}} \frac{g_\alpha}{\text{vol}(\mathcal{G})} \log_2 \frac{\text{vol}(\alpha)}{\text{vol}(\mathcal{G})} \quad (10)$$

where $\text{vol}(\alpha) = \sum_{v \in \mathcal{P}_\alpha} d_v$ is the volume of community \mathcal{C}_α , $d_i^{(\alpha)}$ is the degree of node i in \mathcal{C}_α and g_α is the sum of degrees crossing from \mathcal{C}_α to other communities.

The first term is the **intra-community entropy**, describing the uncertainty of locating a node within its community given the walker is in \mathcal{C}_α :

$$H \left(\left\{ \frac{d_i^{(\alpha)}}{\text{vol}(\alpha)} \right\} \right) = - \sum_{i=1}^{n_\alpha} \frac{d_i^{(\alpha)}}{\text{vol}(\alpha)} \log_2 \frac{d_i^{(\alpha)}}{\text{vol}(\alpha)} \quad (11)$$

The second term measures the **inter-community entropy**, i.e., the cost of describing which community the walker is in. This includes a penalty for community boundary size g_α , effectively discouraging communities with weak modularity or noisy boundaries.

Thus, during entropy minimization, a low-level community \mathcal{C}_α is chosen not merely to cluster adjacent nodes, but to: - Minimize internal entropy by concentrating walk probability on structurally coherent nodes; - Minimize boundary cost g_α , ensuring the community is isolated under random walk dynamics; - And globally reduce the overall coding length of paths on \mathcal{G} . This gives rise to low-level communities that are both **locally tight** and **globally consistent**, satisfying structural objectives beyond local adjacency. Importantly, since g_α and $\text{vol}(\alpha)$ are both computed relative to $\text{vol}(\mathcal{G})$, each community even at the low-level is evaluated in a **global context**. Hence, low-level communities are globally optimized compression units of random walk behavior, fundamentally distinct from simple neighborhood clusters.

In summary, we leverage the low-level communities of the encoding tree as the basis for high-quality topological context construction, and perform leaf-level sampling within them to facilitate graph structure optimization with both local and global insight.

C Existing GSL Paradigms

The existing graph structure learning models can be broadly classified into two paradigms: **Coupled** and **Decoupled**. Below, we will analyze these two paradigms and discuss which one should be adopted for new graph structure learning in the era of LLMs.

Coupled Paradigm. The graph learner and backbone are tightly coupled [2, 6, 28] to learn improved structure by specific downstream tasks (e.g., node, link, and graph level). *Limitations:* (1) *Unstable Performance:* This task- and

backbone-specific model architecture may limit the generalizability of the improved structure and raise fairness concerns due to the potential data quality issues. (2) *Inflexible Deployment*: Switching the downstream backbone or task requires retraining, which significantly limits its adaptability and scalability.

Decoupled Paradigm. The graph learner and downstream backbone are trained independently [18, 16, 1], avoiding co-training, thereby enabling better compatibility with LLMs for GSL. We observe that recent LLM-based GSL methods also tend to adopt this decoupled paradigm [7, 31]. *However, these methods exhibit a different form of coupling (i.e., fine-tuning based on the pre-defined instruction datasets), which leads to the following issues:* (1) They fail to directly and jointly incorporate topology and text, relying instead on instruction datasets. Moreover, they are highly sensitive to the quality of these datasets. (2) They rely on complex mechanisms and significant time to construct instruction datasets and fine-tuning. Therefore, from a model design perspective, we recommend adopting a comprehensive decoupled paradigm to integrate GSL and LLMs, minimizing reliance on fine-tuning and instead prioritizing more efficient and reliable inference with high-quality in-context prompts.

D Empirical Study

In this section, we demonstrate why our proposed tree-based GSL optimization pipeline outperforms other well-trained edge predictor-based methods through node classification experiments on the Citeseer dataset. Specifically, we compare the structure improvement quality of LLaTA against 7 prevalent traditional GSL methods and 2 recent LLM-based GSL methods using 3 metrics: Accuracy, Over-Smoothing, and Over-Squashing.

Accuracy. An intuitive method to evaluate the quality of the improved graph structure is to directly compare the downstream performance. In our implementation, we use a 2-layer GCN to perform node classification, with the resulting accuracy serving as a measure of improved structure.

Over-smoothing and Over-squashing. They are two common challenges in graph learning [21, 34]. Specifically, over-smoothing occurs when node features become indistinguishable as they converge to similar values, while over-squashing arises when nodes fail to capture information from distant neighbors, particularly in the presence of local bottlenecks in the graph. Both issues are strongly tied to the quality of the graph structure. To evaluate graph structure quality in light of these challenges, we employ the following analysis method: To begin with, we train a GCN on the improved graph to generate node embeddings. Then, we compute over-smoothing and over-squashing values by randomly sampling several node pairs: (1) Over-smoothing: We randomly sample 100 pairs of heterophilous nodes and compute their average cosine similarity based on the GCN-generated node embeddings. (2) Over-squashing: We randomly sample 100 pairs of distant homophilous nodes and compute their average cosine similarity using the same embeddings.

The experimental results are presented in Fig.1(d) in Sec.3 of the main text. In our reports, higher accuracy (\uparrow) reflects the improved performance of the downstream GNN on the enhanced graph. Lower over-smoothing (\downarrow) values indicate that the improved graph better distinguishes nodes of different classes, enabling the GNN to learn more discriminative node embeddings. Higher over-squashing (\uparrow) values suggest that the improved graph establishes more connections between distant homophilous nodes, enhancing the model’s ability to capture information from long-range node pairs. According to the experimental results, our proposed decoupled and training-free LLaTA achieves the best performance across all three metrics, demonstrating the effectiveness of the tree-based GSL optimization pipeline compared to other well-trained edge predictor-based methods. Furthermore, we observe that LLM-based GSL methods often outperform traditional GSL approaches, highlighting the importance of developing effective GSL frameworks with text-processing capabilities in the era of LLMs for TAGs.

E Algorithm

E.1 Structural Entropy Minimization

To effectively capture and utilize graph topology, we propose a structural entropy minimization algorithm to obtain a structural encoding tree. This tree reorganizes the graph through the hierarchical structure, simulating its topology evolution. Building upon this, we generate tree-based high-quality prompts for reliable inference, addressing the challenges posed by the absence of fine-tuning. This section provides a detailed overview of the proposed algorithm, along with the fundamental operations involved. The definitions of the three fundamental operations are as follows:

Definition 3. Node Initializing. Consider a node-wise TAG $\mathcal{G} = (\mathcal{V}, \mathcal{E})$ and a root node λ in structural encoding tree \mathcal{T} . Let v be a node in \mathcal{G} . Node Initializing $\text{NI}_{\mathcal{T}}(v, \alpha)$ create node α for v with $\mathcal{P}_{\alpha}^{\text{tree}} = v$ and $\alpha^+ = \lambda$.

Definition 4. Node Combining. Consider an encoding tree \mathcal{T} for $\mathcal{G} = (\mathcal{V}, \mathcal{E})$, and let α and β be two nodes in \mathcal{T} that share the same parent γ . Node combining $\text{NC}_{\mathcal{T}}(\alpha, \beta)$ can be represented as: $\gamma \leftarrow \phi^+$; $\phi \leftarrow \alpha^+$; $\phi \leftarrow \beta^+$. Here, ϕ replaces γ as the new parent of α and β .

Definition 5. Node Lifting. Consider an encoding tree \mathcal{T} for $\mathcal{G} = (\mathcal{V}, \mathcal{E})$, and let α , β and γ be the nodes in \mathcal{T} , satisfying $\alpha^+ = \beta$ and $\beta^+ = \gamma$. Node Lifting $\text{NL}_{\mathcal{T}}(\alpha, \beta)$ can be represented as: $\gamma \leftarrow \alpha^+$; IF $\mathcal{P}_{\beta}^{\text{tree}} = \emptyset$, `delete`(β). Here, α is lifted to the same height as its parent node β , and if β has no children after the lifting, it is removed from \mathcal{T} .

Based on this, the core of our employed greedy algorithm is as follows: (1) Initialization. The structural encoding tree is initialized with 1 height. Then, a root node is created and each original graph node is a leaf node. (2) Node Combination. Pairs of nodes in the tree are iteratively combined to minimize $\mathcal{H}^{\mathcal{T}}(\mathcal{G})$ at each step. This process continues until the root node has at most two children. (3) Node Lifting. Nodes are iteratively lifted to minimize $\mathcal{H}^{\mathcal{T}}(\mathcal{G})$ after each operation. This process is repeated until the tree height is reduced to K , resulting in a final encoding tree \mathcal{T}^K with height K .

The pseudo-code of the high-dimensional structural entropy minimization algorithm is shown in Algorithm E.1.

Algorithm 1: Structural Entropy Minimization

```

1 Input: A graph  $\mathcal{G}$ , the height of encoding tree  $K$ .
2 Output: Encoding tree  $\mathcal{T}^K$  with height  $K$ .
3 // Initialize encoding tree  $\mathcal{T}$  with height 1
4 Create root node  $\lambda$ ;
5 for  $v_i \in \mathcal{V}$  do
6    $\text{NI}_{\mathcal{T}}(v_i, \alpha_i)$  according to Definition. 3;
7 // Node combining
8 while  $\lambda$  has more than 2 children do
9   Select  $\alpha$  and  $\beta$  in  $\mathcal{T}$ , conditioned on  $\alpha^+ = \beta^+ = \lambda$  and  $\arg \max_{\alpha, \beta} \left( \mathcal{H}^{\mathcal{T}}(\mathcal{G}) - \mathcal{H}_{\text{NC}_{\mathcal{T}}(\alpha, \beta)}^{\mathcal{T}}(\mathcal{G}) \right)$ ;
10   $\text{NC}_{\mathcal{T}}(\alpha, \beta)$  according to Definition. 4;
11 // Node lifting
12 while  $\text{height}(\mathcal{T}) > K$  do
13   Select non-root nodes  $\alpha$  and  $\beta$  in  $\mathcal{T}$ , conditioned on  $\alpha^+ = \beta$  and
14    $\arg \max_{\alpha, \beta} \left( \mathcal{H}^{\mathcal{T}}(\mathcal{G}) - \mathcal{H}_{\text{NL}_{\mathcal{T}}(\alpha, \beta)}^{\mathcal{T}}(\mathcal{G}) \right)$ ;
15    $\text{NL}_{\mathcal{T}}(\alpha, \beta)$  according to Definition. 5;
16 Return  $\mathcal{T}^K \leftarrow \mathcal{T}$ ;
```

The structural entropy minimization algorithm reorganizes the graph into a hierarchical encoding tree, minimizing structural entropy to capture topological patterns. Through operations like Node Initializing, Node Combining, and Node Lifting, the algorithm refines the tree by combining nodes and adjusting their positions to reduce entropy. The final tree provides high-quality prompts for reliable inference, enhancing graph structure learning without fine-tuning, and improving efficiency for various tasks.

E.2 Tree-based Adaptive Clustering

To optimize the structural encoding tree obtained by Appendix E.1 using text-driven node features, we introduce an adaptive clustering approach based on tree structures and the silhouette coefficient. This method reallocates leaf nodes according to text-driven insights from LLMs. By maximizing homophily within communities, we ensure that nodes with similar label classes are effectively grouped, aligning with structural patterns commonly observed in real-world applications. For graphs exhibiting heterophily, which are less common but still present, recent studies have demonstrated that uncovering their intrinsic higher-order homophilous patterns is an effective strategy [4, 5, 24].

Specifically, we first initialize the leaf-community clusters using the original structural encoding tree. Based on this, we perform adaptive clustering by silhouette coefficient. The core intuition is to maximize homophily within low-level communities, ensuring that nodes within the same community predominantly belong to the same label class. In other words, (1) it considers the majority label classes within each low-level community, reallocating minority-class leaf nodes; and (2) it leverages the silhouette coefficient to adaptively increase clusters, thereby creating new low-level communities that enhance the tree’s ability to reveal potential homophily patterns.

The following part provides a detailed explanation of this adaptive clustering approach, which enhances the tree’s capability to uncover potential homophily patterns. The pseudo-code of the proposed tree-based adaptive clustering algorithm is presented in Algorithm E.2.

Algorithm 2: Tree-based Adaptive Clustering

```

1 Input: Encoding tree  $\mathcal{T}$ , soft labels  $\mathbf{Y}^{cls}$  for each leaf node, hyperparameter  $s$ .
2 Output: Optimized encoding tree  $\mathcal{T}^*$ .
3 for  $\mathcal{C}^\ell \in \mathcal{T}$  do
4   Let  $\mathbf{Y}_{\mathcal{C}^\ell}^{cls} = \{y_1^{cls}, y_2^{cls}, \dots, y_m^{cls}\}$  be the soft labels of all nodes in  $\mathcal{C}^\ell$ ;
5   Let  $k^* = 0$  and  $sil_{max} = -1$ ;
6   for  $2 < k < \frac{m}{2}$  do
7     Perform k-means( $\mathbf{Y}_{\mathcal{C}^\ell}^{cls}, k$ ) and calculate average silhouette coefficient  $sil_k$  of all clusters;
8     if  $sil_k - sil_{max} < s$  then
9       break;
10    else
11       $sil_{max} = sil_k; k^* = k$ ;
12  Perform k-means( $\mathbf{Y}_{\mathcal{C}^\ell}^{cls}, k^*$ ) and get a set of clusters  $\{C_1, C_2, \dots, C_{k^*}\}$ ;
13  for  $C_i \in \{C_1, C_2, \dots, C_{k^*}\}$  do
14    if  $|C_i| > 1$  then
15      Construct the leaf nodes in  $C_i$  as a new community and set the parent node of the new community to be
16      the same as the parent node of  $\mathcal{C}^\ell$ ;
17    else
18      Reallocate the leaf node in  $C_i$  to other low-level communities based on  $\mathbf{Y}^{cls}$ ;
19 Return  $\mathcal{T}^* \leftarrow \mathcal{T}$ ;

```

In Algorithm E.1, \mathcal{C}_i is the low-level community, m is the number of nodes in \mathcal{C}_i , C_i denotes the i -th cluster in the k-means result, k^* is the best number of clusters, sil_{max} is the current maximum average silhouette coefficient, and s is a hyperparameter and is typically a small value.

Based on the adaptive clustering approach described above, we have optimized the structural encoding tree by reallocating leaf nodes using text-driven node features. In experiments, this method significantly enhanced the homophily within the graph structure. By maximizing homophily within communities, we effectively grouped nodes with similar label classes, improving the expressiveness of the graph structure and resulting in higher accuracy and generalization in graph learning tasks. Specifically, for graphs exhibiting heterophily, we successfully modeled the higher-order homophilic patterns, demonstrating the method’s robustness in handling complex graph structures.

E.3 Leaf-oriented Two-step Sampling

To efficiently reconstruct edge connections from the tree, we propose leaf-oriented two-step sampling. This approach balances running efficiency and practical performance by carefully selecting the subset of leaf nodes. Specifically, this method consists of two key phases: first, it identifies nodes that require optimization by analyzing their topological properties within the graph structure; second, it selects candidate nodes based on semantic similarity to enhance connectivity. By strategically adding or removing edges between these nodes, the method enables effective, training-free

GSL, enhancing the representation quality without additional model fine-tuning. The pseudo-code of the proposed leaf-oriented two-step sampling method is detailed in Algorithm E.3.

Algorithm 3: Leaf-oriented Two-step Sampling

```

1 Input: Original Graph  $\mathcal{G}$ , Optimized encoding tree  $\mathcal{T}^*$ , soft label  $\mathbf{Y}^{cls}$  for each leaf node, hyperparameters  $\theta, r$ .
2 Output: Optimized graph  $\mathcal{G}^*$ .
3 for  $\mathcal{C}^\ell \in \mathcal{T}^*$  do
4   for  $i = 1$  to  $m \times r$  do
5     // Step 1: Sample a leaf node  $\alpha$  from  $\mathcal{C}^\ell$ 
6     Let  $set_1 = \{\alpha | \alpha \in \mathcal{C}^\ell\}$ ;
7     for  $\alpha \in set_1$  do
8       Compute  $\mathcal{H}^{\mathcal{T}^*}(\mathcal{G}, \alpha)$  according to Eq. (9);
9       Compute  $\mathcal{P}_{topo}(\alpha)$  according to Eq. (6);
10    Sample a leaf node  $\alpha$  based on  $\mathcal{P}_{topo}(\alpha)$  from  $set_1$ ;
11    // Step 2: Sample an edge for  $\alpha$ 
12    Let  $set_2 = \{\beta | \beta \in \mathcal{C}^\ell \text{ and } \beta \neq \alpha\}$ ;
13    if  $|set_2| < \theta$  then
14      // Expand the candidate set
15      Let  $\phi$  be the grandparent of  $\alpha$ ;
16      for  $\gamma \in \phi$  and  $\gamma \neq \alpha^+$  do
17        Compute  $y_\gamma^{cls} = \frac{1}{m} \sum_{\alpha \in \gamma} y_\alpha^{cls}$ ;
18        Compute  $\text{sim}(y_\gamma^{cls}, y_\alpha^{cls})$  according to Eq. (3);
19      for  $|set_2| < \theta$  do
20        Choose low-level community with highest sim and add its children to  $set_2$ ;
21    for  $\beta \in set_2$  do
22      Compute  $\text{sim}(y_\beta^{cls}, y_\alpha^{cls})$  according to Eq. (3);
23      Compute  $\mathcal{P}_{sema}^\alpha(\beta)$  according to Eq. (7);
24    if  $|set_2| > \theta$  then
25      Keep the top  $\theta$  nodes in  $set_2$  based on the soft label similarity with  $\alpha$ .
26    For edge addition, sample a leaf node  $\beta$  from  $set_2$  based on  $\mathcal{P}_{sema}^\alpha(\beta)$  ranked in descending order;
27    For edge removal, sample a leaf node  $\beta$  from  $set_2$  based on  $\mathcal{P}_{sema}^\alpha(\beta)$  ranked in ascending order;
28    Add edge to or remove edge from graph  $\mathcal{G}$ ;
29 Return  $\mathcal{G}^* \leftarrow \mathcal{G}$ ;

```

The leaf-oriented two-step sampling method optimizes edge connections by first identifying nodes that require optimization based on their topological properties, ensuring that critical parts of the graph are prioritized for enhancement. In the second phase, candidate nodes are selected using semantic similarity to improve connectivity, focusing on nodes that are contextually relevant. This approach strikes a balance between computational efficiency and practical performance, enabling effective graph structure learning without the need for training. By incorporating both topological and semantic insights, the method refines the graph’s structure, improving its representation quality while ensuring robustness, adaptability, and minimal computational overhead for various graph tasks.

F Theorem Proof

In this section, we provide proofs for all theorems stated in the main text.

F.1 Topological Information Capturing Capability of the Encoding Tree

Theorem 1 (Topological Information Capturing Properties of Encoding Tree). *Given an encoding tree \mathcal{T} and a non-leaf node $\phi \in \mathcal{T}$, the error of topological information $\varepsilon^h(\phi)$ in community \mathcal{C}_ϕ is upper bounded by: $\frac{g_\phi}{2m} \log_2 \frac{\text{vol}(\phi^+)}{g_\phi}$, and $\varepsilon^h(\phi)$ gradually decreases as the community level descends.*

Proof. We partition the proof into two components: (i) derivation of the upper bound for topological information error, and (ii) demonstration of error variation across community hierarchy levels.

Part 1: Upper Bound on Topological Information Error

Suppose a network $\mathcal{G} = (\mathcal{V}, \mathcal{E})$ is given, along with an encoding tree \mathcal{T} of height K . Let ϕ be a non-leaf node (community) in \mathcal{T} located at level k , and denote the corresponding community as $\mathcal{V}_\phi \subseteq V$. Let $\mathcal{G}_\phi = (\mathcal{V}_\phi, \mathcal{E}_\phi)$ be the actual subgraph induced by the community \mathcal{C}_ϕ . Then, the *topological information error* $\varepsilon^h(\phi)$ is defined as the absolute difference between the true structural entropy of the subgraph \mathcal{G}_ϕ and the approximate structural entropy derived from the encoding tree representation:

$$\varepsilon^h(\phi) = |\mathcal{H}(\mathcal{G}_\phi) - \mathcal{H}^\mathcal{T}(\mathcal{G}, \phi)|, \quad (12)$$

where $\mathcal{H}(\mathcal{G}_\phi)$ denotes the optimal value of structural entropy for the true subgraph \mathcal{G}_ϕ , $\mathcal{H}^\mathcal{T}(\mathcal{G}, \phi)$ denotes the local structural entropy corresponding to community ϕ as defined by the encoding tree \mathcal{T} .

First, since the true structural entropy $\mathcal{H}(\mathcal{G}_\phi)$ is defined based on the optimal internal sub-community partitioning, it must be less than or equal to the entropy under a completely random structure. In the worst case, if the internal structure of community ϕ is entirely random, the upper bound of its true structural entropy is:

$$\mathcal{H}(\mathcal{G}_\phi) \leq -\frac{g_\phi}{2m} \log_2 \frac{g_\phi}{\text{vol}(\phi^+)} \quad (13)$$

The intuition here is that when the internal structure of community ϕ is entirely random, the uncertainty of a random walk entering community ϕ reaches its maximum, resulting in the highest possible entropy.

On the other hand, the structural entropy defined by the encoding tree \mathcal{T} is given by:

$$\mathcal{H}_\mathcal{T}(\mathcal{G}; \phi) = -\frac{g_\phi}{2m} \log_2 \frac{\text{vol}(\phi)}{\text{vol}(\phi^+)} \quad (14)$$

Now, we consider the worst-case scenario, that is, the difference between the maximally random structure (with highest entropy) and the simplified approximation provided by the tree (with smaller entropy). Substituting the expressions in Eq. 12 according to Eq. 13 and Eq. 14, we obtain:

$$\varepsilon^h(\phi) = |\mathcal{H}(\mathcal{G}_\phi) - \mathcal{H}_\mathcal{T}(\mathcal{G}; \phi)| \leq \left| -\frac{g_\phi}{2m} \log_2 \frac{g_\phi}{\text{vol}(\phi^+)} + \frac{g_\phi}{2m} \log_2 \frac{\text{vol}(\phi)}{\text{vol}(\phi^+)} \right| \quad (15)$$

Simplifying the expression, we get:

$$\varepsilon^h(\phi) \leq \frac{g_\phi}{2m} \left| \log_2 \frac{\text{vol}(\phi)}{g_\phi} \right| \quad (16)$$

Since for any community ϕ , it always holds that $\text{vol}(\phi) \geq g_\phi$ (as the volume of a community must be greater than or equal to the number of its external edges), we can further loosen the bound by replacing $\text{vol}(\phi)$ with the larger and more general parent volume $\text{vol}(\phi^+) \geq \text{vol}(\phi)$, yielding a broader upper bound:

$$\varepsilon^h(\phi) \leq \frac{g_\phi}{2m} \log_2 \frac{\text{vol}(\phi^+)}{g_\phi} \quad (17)$$

This forms the desired expression for the upper bound of the topological information error in the Theorem. 1.

Part 2: Error Decay Across Hierarchical Community Levels

In this part, we prove that the topological information error becomes progressively smaller as we descend into lower layers (finer communities) of the partitioning tree.

Lemma 1 (Locality and Additivity of Structural Entropy[13]). *Let $\mathcal{G} = (\mathcal{V}, \mathcal{E})$ be a network and let \mathcal{T} be a hierarchical encoding tree of \mathcal{G} . For any non-leaf node $\phi \in \mathcal{T}$ with children β_1, \dots, β_c , the structural entropy of the subgraph \mathcal{G}_ϕ induced by community \mathcal{C}_ϕ satisfies:*

$$\mathcal{H}(\mathcal{G}_\phi) = \sum_{i=1}^c \mathcal{H}(\mathcal{G}_{\beta_i}) + \mathcal{H}^{\text{cross}}(\phi), \quad \mathcal{H}^{\text{cross}}(\phi) = -\sum_{i=1}^c \frac{g_{\beta_i}}{2m} \log_2 \frac{\text{vol}(\beta_i)}{\text{vol}(\phi)} \quad (18)$$

where $\mathcal{H}^{\text{cross}}(\phi)$ is the cross-community contribution that accounts for the uncertainty incurred when identifying sub-communities within \mathcal{C}_ϕ .

Let ϕ be a community at height k in the tree \mathcal{T} , and let its children be β_1, \dots, β_c . In Eq. 12, we define the topological information error as: $\varepsilon^h(\phi) = |\mathcal{H}(\mathcal{G}_\phi) - H_{\mathcal{T}}(\mathcal{G}, \phi)|$.

Expand the first term of the error using Lemma 1:

$$\varepsilon^h(\phi) = \left| \sum_{i=1}^c \mathcal{H}(\mathcal{G}_{\beta_i}) + \mathcal{H}^{\text{cross}}(\phi) - H^{\mathcal{T}}(\mathcal{G}, \phi) \right|. \quad (19)$$

Applying the **triangle inequality**, we obtain an upper bound:

$$\varepsilon^h(\phi) \leq \left| \sum_{i=1}^c (\mathcal{H}(G_{\beta_i}) - H^{\mathcal{T}}(G; \beta_i)) \right| + \mathcal{H}^{\text{cross}}(\phi). \quad (20)$$

To rigorously demonstrate that the error decreases as we move to lower levels (smaller k), we analyze the two terms contributing to the error:

1. **Local structure approximation error** $|\sum_{i=1}^c (\mathcal{H}(G_{\beta_i}) - H^{\mathcal{T}}(G; \beta_i))|$:

For each child community β_i , the local approximation error satisfies the following upper bound (as established in part 1):

$$|\mathcal{H}(G_{\beta_i}) - H^{\mathcal{T}}(G; \beta_i)| \leq \frac{g_{\beta_i}}{2m} \left| \log_2 \frac{\text{vol}(\beta_i)}{g_{\beta_i}} \right|. \quad (21)$$

As we move to lower-level communities (i.e., smaller k), both $\text{vol}(\beta_i)$ and g_{β_i} decrease due to finer partitions and reduced external connectivity. Thus, each term on the right-hand side of Eq. 21 becomes smaller, and so does their sum.

2. **Cross-community entropy term** $\mathcal{H}^{\text{cross}}(\phi)$:

Recall that the cross-community entropy term in Eq. 18, as we go deeper in the tree (i.e., lower communities), both the volumes and g_{β_i} shrink, making this term smaller. Hence, $\mathcal{H}^{\text{cross}}(\phi)$ also decreases as the community level descends.

Combining the above, since both $|\sum_{i=1}^c (\mathcal{H}(G_{\beta_i}) - H^{\mathcal{T}}(G; \beta_i))|$ and $\mathcal{H}^{\text{cross}}(\phi)$ tend to decrease as we move to lower-level communities in the encoding tree (i.e., toward finer communities), the overall error $\varepsilon^h(\phi)$ also tends to decrease with depth. This supports the claim that topological information error decays along the hierarchical levels. \square

F.2 Global information constraints of the low-level communities

Theorem 2 (Implicit Global Constraints in Low-Level Communities). *In a structural encoding tree \mathcal{T} , each low-level community \mathcal{C}^l captures localized topology but implicitly retains global structure constraints due to the hierarchical, random-walk-based formulation of structural entropy.*

Proof. We partition the proof into two components: (i) low-level communities capture localized topology, and (ii) low-level communities implicitly retains global structure constraints.

Part 1: Low-level Communities Capture Localized Topology

From the definition perspective, the structural entropy of a community $\mathcal{C}_\phi \in \mathcal{T}$ is defined as:

$$\mathcal{H}^{\mathcal{T}}(G, \phi) = -\frac{g_\phi}{2m} \log_2 \left(\frac{\text{vol}(\phi)}{\text{vol}(\phi^+)} \right), \quad (22)$$

where g_ϕ is the sum of the cross-node edges that connect nodes within ϕ to nodes outside ϕ , $\text{vol}(\phi) = \sum_{v \in \phi} \deg(v)$ is the volume of ϕ , and ϕ^+ is the parent of ϕ in the tree. This expression depends only on the volume and cut-size between ϕ and ϕ^+ , rather than direct interaction with distant or global components of the graph.

Moreover, since the low-level community \mathcal{C}_ϕ^ℓ typically satisfy:

$$\text{vol}(\phi) \ll \text{vol}(\phi^+), \quad \text{and} \quad g_\phi \ll g_\lambda = 2m, \quad (23)$$

the entropy term of the low-level community \mathcal{C}_ϕ^ℓ becomes more localized [13].

From the algorithmic perspective, the construction of \mathcal{T} through structural entropy minimization encourages the formation of tightly connected, sparsely separated communities. As a result, communities near the leaves tend to consist of closely connected nodes with minimal external edges.

Therefore, low-level communities, both by definition and by optimization, are structurally biased toward encoding localized topological patterns.

Part 2: Low-level Communities Implicitly Retains Global Structure Constraints

We consider a graph $\mathcal{G} = (\mathcal{V}, \mathcal{E})$ and its stationary random walk process, where transition probabilities are defined by:

$$P_{uv} = \frac{\mathbf{A}(u, v)}{\deg(u)}, \quad \text{and} \quad \pi_u = \frac{\deg(u)}{2m}, \quad (24)$$

where \mathbf{A} is adjacency matrix of \mathcal{G} and \deg is the degree of the node.

Let the encoding tree \mathcal{T} be constructed by minimizing the structural entropy, which reflects the minimum cost of encoding a random walk trajectory under a hierarchical community structure.

The structural entropy is defined as:

$$\mathcal{H}^\mathcal{T}(\mathcal{G}) = \sum_{\phi \in \mathcal{T}, \phi \neq \lambda} \mathcal{H}^\mathcal{T}(\mathcal{G}, \phi) = \sum_{\phi \in \mathcal{T}, \phi \neq \lambda} -\frac{g_\phi}{2m} \log_2 \left(\frac{\text{vol}(\phi)}{\text{vol}(\phi^+)} \right). \quad (25)$$

Now let $\phi^{(k)} = \lambda, \phi^{(k-1)}, \dots, \phi^{(1)} = \phi$ be the path in the tree from the root to a low-level community \mathcal{C}_ϕ^ℓ . Then the random walk conditional entry probability into ϕ given hierarchy is:

$$\mathcal{P}(\text{enter } \phi) = \prod_{i=1}^{k-1} \frac{\text{vol}(\phi^{(i)})}{\text{vol}(\phi^{(i+1)})}. \quad (26)$$

This encodes the fact that the deeper a community lies, the more global decisions influence its encoding, each ratio $\frac{\text{vol}(\phi^{(i)})}{\text{vol}(\phi^{(i+1)})}$ reflects how the random walk transitions between communities at each level.

Thus, the total information needed to encode the walk into ϕ can be defined as the *path entropy*:

$$\mathcal{H}_{\text{path}}^\mathcal{T}(\phi) = -\frac{g_\phi}{2m} \log_2 \left(\frac{\text{vol}(\phi)}{\text{vol}(\phi^{(2)})} \right) + \dots + -\frac{g_{\phi^{(1)}}}{2m} \log_2 \left(\frac{\text{vol}(\phi^{(k-1)})}{\text{vol}(\lambda)} \right) \quad (27)$$

This quantity corresponds to a subset of the full structural entropy $\mathcal{H}_\mathcal{T}^{\text{path}}(\alpha) \subseteq \mathcal{H}_\mathcal{T}(\mathcal{G})$, indicating that it reflects only the contribution of a specific path in the tree, while the full entropy aggregates over all nodes in \mathcal{T} .

From the perspective of path entropy, although only $\mathcal{H}^\mathcal{T}(\mathcal{G}, \phi)$ contributes directly to the total structural entropy in Eq. 25, the encoding of a random walk into ϕ must traverse the full ancestral path $\lambda \rightarrow \phi^{(k-1)} \rightarrow \dots \rightarrow \phi$. Thus, the effective information cost of encoding a transition into ϕ is represented by $\mathcal{H}_{\text{path}}^\mathcal{T}(\phi)$, which includes contributions from all higher-level communities.

Moreover, since \mathcal{T} is obtained by minimizing the total structural entropy $\mathcal{H}^\mathcal{T}(\mathcal{G})$, the $\mathcal{H}_{\text{path}}^\mathcal{T}(\phi)$ is also simultaneously subject to the minimization constraint, which means the division and refinement of communities—including low-level ones—are jointly optimized under global constraints. In particular, each local partition is chosen not independently, but in the context of its position within the tree, as reflected in equation Eq. 27.

Therefore, Even though the structure of ϕ is small and local, its encoding depends on the full sequence of volume and boundary terms from all ancestors $\phi^{(i)}$, which are determined by global topology. Hence, low-level communities capture local topological patterns while implicitly preserving global structural constraints. \square

F.3 The Error Bound Between Soft Labels and True Labels

Theorem 3 (Error Bound Between Soft labels and True Labels). *Given two leaf nodes α and β in \mathcal{T} , the error between soft label similarity and true label similarity is bounded by:*

$\varepsilon^y(\alpha\beta) = |\text{sim}(y_\alpha^{cls}, y_\beta^{cls}) - \text{sim}(y_\alpha, y_\beta)| \leq \delta \cdot (1 - \epsilon)$, where δ is a constant that depends on the LLM's in-context learning ability, y_α is the true label of α and ϵ is the text similarity threshold.

Proof. The proof leverages three key lemmas derived from the Transformer architecture in [25].

Lemma 2 (Attention-Induced Local Homophily). *Let t_α^* be the aggregated text of node α using threshold ϵ (Eq. 2). The raw soft label error $\Delta_\alpha^{raw} = |y_\alpha^{cls} - y_\alpha|$ satisfies:*

$$\Delta_\alpha^{raw} \leq \delta_1 \cdot (1 - \epsilon), \quad (28)$$

where δ_1 depends on the attention weight distribution, and Δ_α^{raw} is the raw prediction error before residual connections and layer normalization, directly generated by the output of the attention mechanism.

Proof. From the scaled dot-product attention mechanism:

$$\text{Attention}(Q, K, V) = \text{softmax}\left(\frac{QK^T}{\sqrt{d_k}}\right)V, \quad (29)$$

the threshold ϵ filters neighbors with $w_{\alpha\beta} \geq \epsilon$ (Eq. 2 and Eq. 3). The multi-head attention reinforces local semantic consistency across subspaces, bounding the error proportionally to $(1 - \epsilon)$ [25]. \square

Lemma 3 (Stability via Residual Connections). *The residual connections and layer normalization compress the error:*

$$\Delta_\alpha \leq \delta_2 \cdot \Delta_\alpha^{raw}, \quad (30)$$

where $\delta_2 < 1$ is a normalization gain factor.

Proof. The residual structure $\text{LayerNorm}(x + \text{Sublayer}(x))$ suppresses feature drift, with d_{model} as the hidden dimension [25]:

$$\|\Delta_\alpha\| \leq \frac{|\Delta_\alpha^{raw}|}{\sqrt{d_{\text{model}}}} \leq \delta_2 \cdot |\Delta_\alpha^{raw}|, \quad (31)$$

where d_{model} is the model dimension. The normalization operation stabilizes training by scaling the gradient direction, reducing the magnitude of error propagation. \square

Lemma 4 (Representation Capacity). *The hidden dimension d_{model} governs semantic precision:*

$$\delta_1 \propto d_{\text{model}}^{-0.5}. \quad (32)$$

Proof. The learning rate design $\text{lr} = d_{\text{model}}^{-0.5} \cdot \min(\cdot)$ indicates that increasing the model dimensionality necessitates a reduction in learning rate to preserve training stability. A larger d_{model} enhances the model's feature representation capacity, while the error decay rate per unit dimension scales proportionally with $d_{\text{model}}^{-0.5}$ [25]. \square

Recall the definition of cosine similarity, the similarity between two vectors is defined as:

$$\text{sim}(x_i, x_j) = \frac{x_i \cdot x_j}{\|x_i\| \|x_j\|} \quad (33)$$

Substituting this into our error analysis yields:

$$\varepsilon^y(\alpha\beta) = \left| \text{sim}(y_\alpha^{cls}, y_\beta^{cls}) - \text{sim}(y_\alpha, y_\beta) \right| = \left| \frac{y_\alpha^{cls} \cdot y_\beta^{cls}}{\|y_\alpha^{cls}\| \|y_\beta^{cls}\|} - y_\alpha \cdot y_\beta \right|. \quad (34)$$

Since the ground truth labels are one-hot encoded, satisfying $\|y_\alpha\| = \|y_\beta\| = 1$, the similarity can be simplified as: $y_\alpha \cdot y_\beta$.

Through **error decomposition** and application of the **triangle inequality**, we obtain:

$$\varepsilon^y(\alpha\beta) \leq \underbrace{\left| \frac{y_\alpha^{cls} \cdot y_\beta^{cls}}{\|y_\alpha^{cls}\| \|y_\beta^{cls}\|} - y_\alpha^{cls} \cdot y_\beta \right|}_{\text{Term 1}} + \underbrace{\left| y_\alpha^{cls} \cdot y_\beta - y_\alpha \cdot y_\beta \right|}_{\text{Term 2}}. \quad (35)$$

Bounding Term 2: Since y_β is one-hot (non-zero at index j):

$$\text{Term 2} = |(y_\alpha^{cls} - y_\alpha) \cdot y_\beta| \leq \Delta_\alpha \cdot |y_\beta| \leq \delta_1 \delta_2 (1 - \epsilon). \quad (\text{By Lemma 2\& 3.}) \quad (36)$$

Lemma 5 (Normalization Perturbation). *For any vectors $u, v \in \mathbb{R}^d$ where v is normalized ($\|v\| = 1$) and $\|u - v\| \leq \eta$, the following inequality holds for their normalized difference:*

$$\left\| \frac{u}{\|u\|} - v \right\| \leq \frac{2\eta}{\|u\|} \leq 2\eta$$

where the second inequality follows from $\|u\| \geq 1 - \eta$ (by the reverse triangle inequality).

Bounding Term 1: Using the vector normalization Lemma 5 with $u = y_\beta^{cls}$ and $v = y_\beta$. if $\|y_\beta^{cls} - y_\beta\| \leq \delta_1 \delta_2 (1 - \epsilon) = \eta$, then:

$$\text{Term 1} \leq \|y_\alpha^{cls}\| \cdot \left\| \frac{y_\beta^{cls}}{\|y_\beta^{cls}\|} - y_\beta \right\| \leq 2\delta_1 \delta_2 (1 - \epsilon). \quad (37)$$

Final Bound: Combining both terms and incorporating Lemma 4:

$$\varepsilon^y(\alpha\beta) \leq 3\delta_1 \delta_2 (1 - \epsilon) \leq \delta \cdot (1 - \epsilon), \quad (38)$$

where $\delta = 3\delta_1 \delta_2 \cdot d_{\text{model}}^{-0.5}$ depends on the in-context learning ability of the LLMs.

In summary, we have proven that the similarity of soft labels y^{cls} generated through our **Community of Thought** mechanism can approximate the similarity of ground-truth labels y with controllable bias ε^y , where this bias decreases as:

- Local homophily threshold ϵ increases (i.e., tighter neighbor selection),
- and LLM in-context learning capacity δ improves (e.g., via larger model size or better training).

□

F.4 Structural Entropy and Node Topological Uncertainty

Theorem 4 (High-Entropy Nodes Require Supervision). *In a structural encoding tree \mathcal{T} constructed via entropy minimization, nodes with higher structural entropy $\mathcal{H}^T(\mathcal{G}, \alpha)$ indicate: higher topological uncertainty within their local structural context.*

Proof. We begin by recalling the definition of structural entropy for a node $\phi \in \mathcal{T}$, derived from the minimum encoding length of a random walk process:

$$\mathcal{H}^T(\mathcal{G}, \phi) = -\frac{g_\phi}{2m} \log_2 \left(\frac{\text{vol}(\phi)}{\text{vol}(\phi^+)} \right), \quad (39)$$

where g_ϕ is the sum of the cross-node edges that connect nodes within ϕ to nodes outside ϕ , $\text{vol}(\phi) = \sum_{v \in \phi} \text{deg}(v)$ is the volume of ϕ , and ϕ^+ is the parent of ϕ in the tree.

Structural entropy encodes the uncertainty of random walk transitions. In the structural entropy formulation, the graph is viewed as a Markov chain, and each term $\mathcal{H}^T(\mathcal{G}, \phi)$ represents the expected number of bits needed to encode a random walker's transition from ϕ^+ into ϕ along a hierarchical path in the encoding tree.

Let us consider the conditional transition probability from ϕ^+ to ϕ , denoted as:

$$P(\phi | \phi^+) = \frac{\text{vol}(\phi)}{\text{vol}(\phi^+)}. \quad (40)$$

The negative log of this transition probability reflects the information content (surprisal) of the walk entering ϕ . When $\text{vol}(\phi)$ is close to $\text{vol}(\phi^+)$, i.e., $P(\phi | \phi^+) \rightarrow 1$, the encoding cost (entropy) becomes small. But when this ratio becomes ambiguous (e.g., many similar-volume subregions), entropy increases.

Moreover, the term g_ϕ acts as a weight reflecting how often the walker exits or enters ϕ . A larger g_ϕ means more random walks intersect the boundary of ϕ , suggesting weaker internal cohesion and a blurrier community boundary.

From the above, the entropy term $\mathcal{H}^T(\mathcal{G}, \phi)$ grows when:

- $\frac{\text{vol}(\phi)}{\text{vol}(\phi^+)} \approx 0.5$, i.e., the walker has nearly equal chance to enter multiple subcommunities;
- g_ϕ is large, i.e., there are many transitions across community boundaries.

In such scenarios, the community ϕ has:

- a **high encoding cost** (random walk description length is large),
- and a **weak structural separability**, because the walker often crosses between α and other regions.

Thus, a node $v \in \mathcal{P}_\phi^{tree}$ inherits this high entropy $\mathcal{H}_T(\mathcal{G}, \phi)$, reflecting the fact that its structural position within the graph is more ambiguous. It is harder to determine whether it coherently belongs to a community based solely on graph structure, and hence it exhibits higher topological uncertainty. \square

Table 6: Details of experimental datasets.

Dataset	# Nodes	# Edges	# Classes	# Train/Val/Test	# Homophily	Text Information	Domains
Cora	2,708	10,556	7	60/20/20	0.81	Title and Abstract of Paper	Citation
Citeseer	3,186	8,450	6	60/20/20	0.74	Title and Abstract of Paper	Citation
Pubmed	19,717	88,648	3	60/20/20	0.80	Title and Abstract of Paper	Citation
WikiCS	11,701	431,726	10	5/22.5/50	0.65	Title and Abstract of Article	Knowledge
Instagram	11,339	144,010	2	10/10/90	0.59	Personal Profile of User	Social
Reddit	33,434	269,442	2	10/10/90	0.59	Last 3 Posts of User	Social
Ratings	24,492	186,100	5	25/25/50	0.38	Name of Product	E-commerce
Child	23,327	240,604	12	60/20/20	0.42	Name and Description of Book	E-commerce
History	41,551	503,180	12	60/20/20	0.64	Name and Description of Book	E-commerce
Photo	48,362	873,793	12	60/20/20	0.74	User Review of Product	E-commerce

G Datasets

We evaluate LLaTA and baselines on 10 widely adopted TAG datasets across multiple domains, including 3 citation networks [3], 1 knowledge network [3], 2 social networks [9], and 4 e-commerce networks [29]. Among these, the Ratings and Child exhibit heterophily, while the remaining datasets follow homophily. The details of these TAG datasets are shown in Table 6. The description of the datasets for each domain is as follows:

- **Citation Networks** [3]. Cora, Citeseer, and Pubmed are benchmark datasets of citation networks. Nodes represent paper, and edges represent citation relationships. The features are obtained through pre-trained language model, and labels denote their academic fields.
- **Knowledge Networks** [3, 20]. WikiCS is a benchmark dataset of knowledge networks. Nodes represent articles in the field of computer science, and edges represent hyperlinks between these articles. The features are obtained through pre-trained language model, and labels denote different branches of computer science.
- **Social Networks** [9]. Instagram and Reddit are benchmark datasets of social networks. Nodes represent users, and edges represent social relationships. The features are obtained through pre-trained language model, and labels correspond to different types of users.
- **E-commerce Networks** [29]. Ratings, Child, History and Photo are benchmark datasets of e-commerce networks. Nodes represent products, and edges represent relationships such as co-purchase or co-view. The features are obtained through pre-trained language model, and labels correspond to product categories or user ratings.

H Baselines

In this section, we provide a brief description for each baseline used in the experiments. It includes 5 coupled GSL methods [2, 6, 32, 28, 37], 6 decoupled GSL methods [11, 18, 14, 16, 21, 1], and 2 LLM-based GSL methods [7, 31]. Based on this, we apply prevalent GCN [12], GAT [26], and GraphSAGE [8] as the downstream backbone. For LLM-based methods, we primarily select GLM-4-9B as the LLM backbone. For LLaTA, we utilize the GLM-4 to perform inference on the node classification probabilities. For LLM4RGNN, we use the GLM-4 to construct the fine-tuning dataset and fine-tune the Llama-3-8B for edge prediction; for GraphEdit, we use the GLM-4 for both fine-tuning and edge prediction.

All baselines are briefly described as follows:

- **GCN** [12]. GCN is among the most widely adopted GNN architectures, as it introduces a first-order approximation of a localized spectral filter for graph-structured data.
- **GAT** [26]. GAT incorporates a self-attention mechanism to compute importance scores for different neighboring nodes, enabling more effective aggregation of neighborhood information.
- **GraphSAGE** [8]. GraphSAGE [14] is an inductive framework that generates node embeddings by leveraging node features and using a sampling-based approach to aggregate information from the local neighborhood, enabling scalable representation learning.
- **IDGL** [2]. IDGL is a framework that learns a refined graph structure by leveraging cosine similarity of features and top-k threshold refinement, combining it with the original graph for joint optimization.
- **SLAPS** [6]. SLAPS is a graph learning framework that uses MLP-based embeddings and kNN to build the graph. The adjacency matrix is symmetrized and normalized, and a self-supervised denoising autoencoder is used to update both the graph and model parameters.
- **GAUGO** [32]. GAUGO uses a graph auto-encoder to learn a new graph structure. It predicts edges based on node features, refines the edge probabilities with Gumbel sampling, and fuses the generated graph with the original one before training. Both the generated graph and model parameters are updated during optimization.
- **HESGSL** [28]. HESGSL uses hierarchical embeddings to capture both local and global graph structures. It employs self-supervised learning with clustering and attention mechanisms to enhance feature representation and performance on downstream tasks.
- **SEGS** [37]. SEGS constructs a graph by fusing a kNN graph with the original graph, leveraging structural entropy and encoding tree to refine edges and hierarchically extract community structures. The graph and model parameters are optimized jointly during training.
- **ProGNN** [11]. ProGNN refines graph structures by enforcing low-rank, sparsity, and similarity constraints, jointly optimizing the learned graph and model parameters without predefined GSL bases or graph fusion.
- **SUBLIME** [18]. SUBLIME constructs GSL graphs using an anchor view (original graph) and a learner view. The learn view is initialized with kNN and optimized with parameterized or non-parameterized methods, followed by post-processing steps like top-k filtering and symmetrization. Contrastive learning between the two views refines the graph for downstream tasks.
- **STABLE** [14]. STABLE employs Graph Contrastive Learning (GCL) to generate robust graphs by perturbing node similarities and edges. Positive samples use slight perturbations, while negative samples use shuffled features. The graph refinement step applies a top-k filtering strategy on the node similarity matrix to retain helpful edges while removing adversarial ones.
- **CoGSL** [16]. CoGSL constructs GSL graphs by combining the original graph with additional views, such as adjacency or kNN graphs. Node embeddings are generated via GCNs, and connection probabilities are estimated and refined using InfoNCE loss to maximize mutual information. The final graph is obtained through early fusion and updated with model parameters.
- **BORF** [21]. BORF is a curvature-based graph rewiring approach aimed at addressing over-smoothing and over-squashing in GNNs. It leverages Ollivier-Ricci curvature to identify edges with extreme curvature values—positive for over-smoothing and negative for over-squashing. This process preserves the graph’s topology while improving message-passing efficiency and enhancing GNN performance on downstream tasks.
- **DHGR** [1]. DHGR enhances GNN performance on heterophily graphs by preprocessing the graph structure through rewiring. It systematically adds homophilic edges and removes heterophilic ones based on label and feature similarities, improving node classification accuracy, particularly for heterophily settings.
- **GraphEdit** [7]. GraphEdit refines graph structures by integrating LLMs with a lightweight edge predictor to enhance graph representation learning. By leveraging instruction-tuning and training edge predictor, GraphEdit effectively denoises noisy connections and identifies implicit relationships among nodes.
- **LLM4RGNN** [31]. LLM4RGNN is a framework that enhances the adversarial robustness of GNNs using LLMs. It detects malicious edges and restores critical ones through a purification strategy, leveraging fine-tuned LLMs for edge prediction and correction. This approach effectively mitigates topology attacks, improving GNN performance across attack scenarios.

I Hyperparameter Settings

For LLaTA and all baselines, we uniformly adopt 2-layer GCN as encoder, the hidden dimensional is set to 64, and dropout (rate=0.5) is applied between GCN layers. The GNN encoder is optimized for 200 epochs using the Adam optimizer, with an initial learning rate of 0.01 and weight decay of $5e-4$. We use early stopping with a patience of 20 epochs on the validation loss. 11 experiments are repeated 10 times with different random seeds, and results are reported as *mean* \pm *std*. We run the code on NVIDIA A100 GPUs with CUDA 11.2.

For LLaTA, the hyperparameters are searched as follows: The height of encoding tree K in Sec. 4.2 is chosen from $\{2, 3, 4, 5\}$, the similarity threshold ϵ in Sec. 4.3 is selected from $[0.4, 0.6]$, while the size of the candidate set θ in Sec. 4.4 is searched in $\{3, 5, 10, 15, 20\}$, and the two-step sampling frequency r is tuned among $\{1, 3, 5, 10, 25\}$.

For other baselines, we primarily adopt the optimal hyperparameters reported in their original papers. If no such configurations are available, we utilize Optuna to automatically determine the best hyperparameter settings for these baselines.

J Case Study

In this section, we conduct experiments on the Citeseer, focusing on a low-level community as a case study to track and visualize the data flow within the LLaTA pipeline. Based on this, we aim to provide a clear and intuitive explanation of our method, particularly focusing on LLM inference. Our goal is to make the process transparent, thereby avoiding the uncontrollable nature of a black-box approach.

Reviewing the three modules of LLaTA (detailed descriptions can be found in Sec. 4.2-4.4), we observe that Step 1: Topology-aware In-context Construction (Sec. 4.2) and Step 3: Leaf-oriented Two-step Sampling (Sec. 4.4) have relatively fixed computation in which LLMs do not actively participate or play a secondary role. This is not directly related to our goal of visualizing the LLM inference through the case study to provide a deeper analysis of LLaTA’s interpretability. Therefore, we focus on Step 2: Tree-prompted LLM Inference (Sec. 4.3), specifically analyzing its three components: *Reception-aware Leaf Augmentation*, *Community of Thought*, and *Leaf Dependency Allocation*. In Fig. 7, we use a low-level community as an example and offer a detailed demonstration of the LLaTA inference.

Reception-aware Leaf Augmentation. After tree initialization by minimizing SE, we aim to construct high-quality, topology-aware in-context for LLM inference. In this process, the quality of node-wise textual information is crucial, as it directly impacts the LLM’s semantical understanding and the confidence of inference results. Therefore, we first perform text propagation and aggregation within each community, guided by the tree, to achieve leaf augmentation. Specifically, we input a low-level community and perform text propagation and aggregation within this community to enrich the text of each node. As illustrated in Fig. 7, we take red node 1 as an example. After text propagation and aggregation, this node acquires the text of red node 2 for enhancement. The text of red node 1 is then combined with that of red node 2 using the following prompt:

Prompt 1 - Part I: Here is a paper 1 which belongs to one of the following categories: Agents, Machine Learning, Information Retrieval, Database, Human-Computer Interaction, Artificial Intelligence.

The description of Agents: This research area encompasses topics such as multi-agent systems, reinforcement learning, and agent-based modeling...

The description of Machine Learning: This research area focuses on developing algorithms that enable systems to learn from data and make predictions or decisions without explicit programming...

The description of ...

Prompt 1 - Part II: The abstract of paper 1: The Computational Theory of Neural Networks In the present paper a detailed taxonomy of neural network models with various restrictions is presented with respect to their computational properties. The criteria of classification include e.g. feedforward and recurrent architectures, discrete...

Prompt 1 - Part III: The abstract of other papers related to its content: A Computational Taxonomy and Survey of Neural Network Models We survey and summarize the existing literature on the computational aspects of neural network models, by presenting a detailed taxonomy of the various models according to their computational characteristics...

Community of Thought. Leveraging the enhanced leaf nodes, we propose a Community of Thought (CoT) prompt mechanism, which incorporates community-enhanced descriptions for each node and its related neighbors, facilitating more reliable LLM inference. Specifically, we combine the previously obtained enhanced textual information (obtained by Prompt 1) with the community-enhanced descriptions and the specific requirements of the inference task (Prompt 2). These combined inputs are then fed into the LLM to predict the probability of the node belonging to each category. Based on the LLM’s output, we apply the softmax function to obtain the node’s soft label, mapping it into the semantic

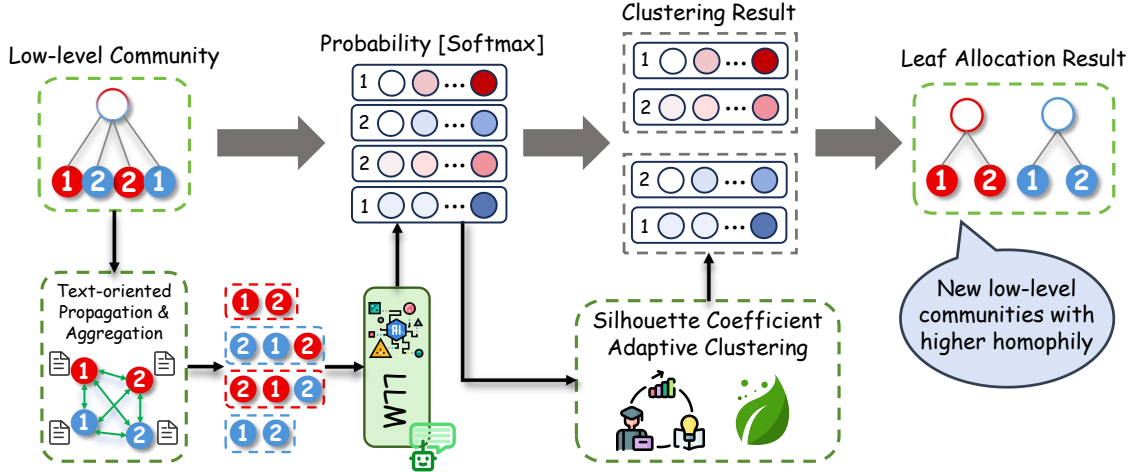


Figure 7: A case study of the tree-prompted LLaTA inference.

vector space encoded by the LLM. As an illustrative example, we present the formulation of Prompt 2, the corresponding LLM output, and the derived soft label for red node 1, as shown below.

Prompt 2: Based on the abstract of paper 1 and other papers, please provide the probability that paper 1 belongs to each category.

For the current paper 1, please focus on the topic, methodology, keywords, and conclusions.

For the related papers, please focus on parts similar to those on paper 1.

Use integers from 0 to 9 to represent the probabilities. 0 means it is impossible to belong to that category, and 9 means it definitely belongs to that category. The example format is: [8, 4, 1, 2, 5, 3].

LLM Answer: The probabilities of paper 1 belonging to each category are: [0, 7, 0, 0, 0, 9].

Soft Label of Red Node 1 [Softmax Function]:
[0.00, 0.12, 0.00, 0.00, 0.00, 0.88].

Leaf Dependency Allocation. Finally, based on the leaf soft labels, we perform silhouette coefficient-based adaptive clustering on the four leaf nodes. As shown in Fig. 7, the clustering results indicate that the two red nodes are grouped into one cluster, while the two blue nodes are assigned to another. Following these clustering results, we reconstruct two new low-level communities to replace the original ones. This process ultimately enhances community homophily and further optimizes the tree through LLM inference.

K LLM Backbone Analysis

Table 7: Performance of LLaTA with different LLM backbones.

LLM	Pubmed	WikiCS	Instagram	History
Llama-2-13B	87.79 \pm 0.31	80.64 \pm 0.32	66.12 \pm 0.21	84.21 \pm 0.28
Llama-3-8B	88.01 \pm 0.33	81.13 \pm 0.29	66.34 \pm 0.21	84.86 \pm 0.35
Mistral-7B	88.07 \pm 0.28	81.02 \pm 0.24	66.29 \pm 0.20	84.98 \pm 0.34
GLM-4-9B	88.39\pm0.23	81.58\pm0.20	66.73\pm0.13	85.28\pm0.24

To further answer Q2, we analyze the performance of LLaTA with different LLM backbones. Specifically, we evaluate the node classification performance of LLaTA with different LLM backbones on four datasets from different domains, with the results presented in Table 7.

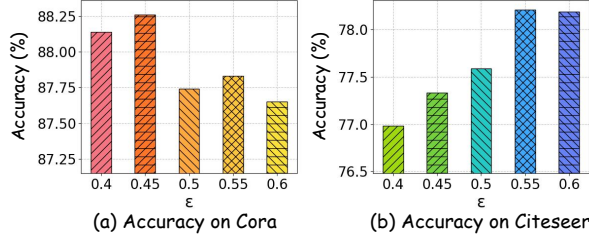


Figure 8: The performance of LLaTA with different ϵ on Cora and Citeseer datasets.

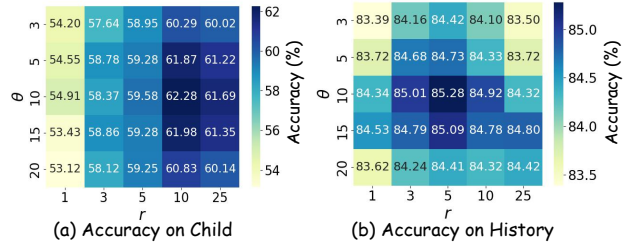


Figure 9: The performance of LLaTA with different θ and r on Child and History datasets.

The experimental results demonstrate that LLaTA performs effectively with different LLM backbones, highlighting the versatility of our method. GLM-4-9B outperforms the other LLM backbones, particularly on the WikiCS and Instagram datasets, due to its stronger in-context learning ability and stable outputs, which lead to higher inference accuracy. In contrast, Llama-2-13B shows the worst performance, especially on WikiCS and History, likely due to its limited ability to grasp complex contextual relationships and output instability. Llama-3-8B and Mistral-7B provide more balanced results, with Mistral-7B offering a good trade-off between efficiency and performance. These findings emphasize that LLaTA can effectively leverage various LLM backbones for downstream tasks. Moreover, the performance differences highlight the importance of strong text inference abilities in LLMs, when combined with GSL to enhance the performance of downstream tasks. Overall, the experimental results demonstrate that LLaTA is a flexible and interpretable method, which effectively integrates LLMs with GSL.

L Hyperparameter Analysis

To further answer **Q3**, we analyze the impact of the similarity threshold ϵ in Sec. 4.3. Additionally, we conducted further analysis on the impact of parameters θ and r in Sec. 4.4 across more datasets.

L.1 Analysis of Hyperparameter ϵ

Specifically, we evaluate the node classification performance of LLaTA under varying ϵ on the Cora and Citeseer, with the results presented in Fig. 8.

The experimental findings indicate that the hyperparameter ϵ is critical in determining the quality of the in-context information provided to LLMs and the effectiveness of their inference. A small ϵ value may lead to the aggregation of nodes from different classes, introducing noise into the in-context and thereby reducing inference accuracy. Conversely, an excessively large ϵ may result in over-filtering, disregarding important connections between similar nodes, ultimately leading to a loss of meaningful relationships and failing to provide high-quality contextual information for LLMs. Our results suggest that an appropriate range for ϵ is between 0.4 and 0.6, which balances the trade-off between minimizing noise and preserving essential connections. Specifically, the optimal ϵ value is 0.45 for Cora and 0.55 for Citeseer. In conclusion, the selection of an appropriate ϵ value plays a critical role in constructing high-quality in-context information for LLMs, ultimately enhancing the overall performance and robustness of LLaTA across diverse tasks and datasets.

L.2 Analysis of Hyperparameters θ and r

To thoroughly analyze the impact of θ and r on LLaTA’s performance, we conducted additional experiments on the Child and History datasets, with the results presented in Fig. 9.

Our evaluation on the Child dataset shows pronounced sensitivity to the two-step sampling frequency r . Accuracy peaks at $r = 10$ (62.28%) before declining to 61.69% at $r = 25$, confirming that excessive edge additions ($r \geq 25$) disrupt heterophilic structures. The semantic sampling parameter θ maintains stable performance (61.87%-61.98%) within $[5, 15]$, while extreme values ($\theta = 3$ or 20) cause 1-2% drops due to sampling limitations. The History dataset demonstrates LLaTA’s robustness to r variations (84.32%-85.28% accuracy), with only 0.02% difference between $r = 5$ (85.34%) and $r = 25$ (85.32%). For θ , peak accuracy at $\theta = 10$ (85.28%) varies by less than 1% across $[5, 15]$. This systematic comparison reveals that θ optimization should be performed after determining r , particularly for heterophilic graphs where r significantly impacts structural integrity while θ mainly affects sampling quality.

Table 8: Complete runtime(h) results of LLaTA across all 10 datasets.

Method	Cora	Citeseer	Pubmed	WikiCS	Instagram	Reddit	Ratings	Child	History	Photo
LLaTA _{G_{GN}}	1.593	1.974	11.872	7.081	6.850	20.136	14.583	14.016	25.394	29.373
LLaTA _{G_{AT}}	2.592	2.974	12.871	8.080	7.849	21.138	15.583	15.014	26.393	30.369
LLaTA _{S_{AGE}}	3.594	3.975	13.875	9.085	8.852	22.139	16.588	16.016	27.398	31.341

These findings collectively validate the dataset-dependent nature of r 's impact and the universal stability of θ observed in our primary experiments. The Child dataset's heterophily demands careful r calibration to avoid overhomophilization, whereas History's homophily permits broader parameter flexibility. Both datasets corroborate that $\theta \in [5, 15]$ serves as a reliable default range, though practitioners should prioritize r tuning when deploying LLaTA on heterophilic graphs. The consistent performance patterns across three distinct graph types (Cora, Child, History) strengthen the generalizability of our parameter guidelines.

M Efficiency Analysis of LLaTA

In this section, we present the complete runtime performance of LLaTA across 10 tagged datasets in Table 8, along with a comprehensive analysis of our method's computational efficiency advantages.

Current graph structure learning (GSL) methods face significant efficiency bottlenecks, particularly in large-scale or noisy graphs. Traditional approaches—including metric learning, probabilistic modeling, and direct optimization—often require computationally expensive pairwise similarity calculations (e.g., kernel functions or attention mechanisms) or iterative optimization of adjacency matrices[36]. These operations exhibit quadratic or higher complexity relative to node counts, limiting scalability. For LLM-based GSL Methods (e.g., GraphEdit [7], LLM4RGNN [31]), efficiency issues are further exacerbated by the inherent overhead of large-model inference and fine-tuning. Empirical results reveal that these methods exceed 72 hours on larger datasets among the 10 benchmarks (As shown in Table 1), primarily due to their reliance on full-parameter tuning and dense graph operations.

Compared to existing paradigms, our framework achieves superior efficiency by: **(a) Topology-Aware Context Enhancement:** The Community-of-Thought mechanism provides high-quality topological context to guide LLM reasoning, eliminating the need for fine-tuning. By leveraging the inherent structure-awareness of communities, we reduce the dependency on costly end-to-end training while improving inference accuracy. **(b) Parameter-Free Structure Reconstruction:** A tree-based sampler enables lightweight graph restructuring without trainable parameters. This avoids the computational overhead of gradient-based adjacency matrix optimization (e.g., nuclear norm regularization in ProGNN [11]) or probabilistic sampling (e.g., Gumbel-Softmax in NeuralSparse [33]).

Enabled by these two key innovations, our framework achieves superior efficiency by: **(1) Eliminating Fine-Tuning:** Bypassing LLM parameter updates reduces GPU memory and time costs by orders of magnitude. **(2) Sublinear Complexity:** The tree sampler operates locally within communities, avoiding global pairwise calculations. **(3) Parallelizability:** Community-level operations enable distributed processing, scaling to graphs with 10^{5+} nodes where baseline LLM-GSL methods fail.